Ore Geology Reviews 158 (2023) 105465

Contents lists available at ScienceDirect

Ore Geology Reviews

journal homepage: www.elsevier.com/locate/oregeorev

Review

Processes of magmatic sulfide mineralization of the Huangshan-Jingerquan Ni-Cu metallogenic belt, NW China: Insights from reviews of chalcophile elements

Xie-Yan Song [a,*], Wei Xie [b], Yu-Feng Deng [c], Jian Kang [a,d], Kai-Yuan Wang [e], Wen-Qin Zheng [a]

[a] State Key Laboratory of Ore Deposit Geochemistry, Institute of Geochemistry, Chinese Academy of Sciences, Guiyang 550081, PR China
[b] College of Oceanography, Hohai University, Nanjing 210098, PR China
[c] Ore Deposit and Exploration Center (ODEC), Hefei University of Technology, Hefei, Anhui 230009, PR China
[d] University of Chinese Academy of Sciences, Beijing 100039, PR China
[e] School of Earth Sciences of Engineering, Hebei University of Technology, PR China

ARTICLE INFO

Keywords:
Ni-Cu sulfide metallogenic belt
Magma plumbing system
Platinum-group element
Sulfide liquid differentiation
Orogenic belt
China

ABSTRACT

The Ni-Cu sulfide deposits along the Huangshan-Jingerquan metallogenic belt in the southernmost Central Asian Orogenic Belt contain ~ 1.0 million tonnes Ni metal with average grades of 0.4–0.5 wt%. Published data on siderophile and chalcophile elements of sulfide ores and sulfide-poor rocks of the deposit hosting complexes are integrated to address the processes affecting compositions of the sulfide ores, such as sulfide segregation, differentiation and mixing. The sulfide-poor rocks are low in platinum-group elements (PGE), e.g. Ir < 0.23 ppb and Pd < 2.3 ppb, even containing minute amount of sulfides. These data indicated that the basaltic magmas were primarily depleted in PGE due to sulfide retention in the mantle sources or in the lower crust. Abundances and variation of PGE of the sulfide-poor rocks indicate that fractional crystallization of olivine, pyroxene and chromite lead to fractionation of Ir and Ru from Pt and Pd in the basaltic magmas ascending in the crust. The disseminated sulfide ores with S < 3.0 wt% from the deposits have restricted PGE tenors (0.5–45 ppb Ir, 10–900 ppb Pt and 10–780 ppb Pd) and Pd/Ir values (3.0–250), whereas the net-textured/massive ores have relatively large variations in PGE tenors (0.05–55 ppb Ir, 0.4–2900 ppb Pt and 4.0–2560 ppb Pd) and Pd/Ir values (0.3–4000). Large compositional variations of the net-textured/massive ores demonstrate differentiation and mixing of the sulfide liquids carried by different batches of magma along the magma plumbing system. The sulfides settled down in widen parts of magma conduits forming sulfide mineralized mafic–ultramafic dykes. Downward percolation of differentiated sulfide liquids could form Fe-rich and Cu-rich massive ore veins adjacent to dyke-like orebody. More sulfides were carried by ascending magmas and deposited in shallow large complexes along the magma plumbing system.

1. Introduction

Different size Ni-Cu sulfide deposits occur in orogenic belts over the world, such as the Kotalahti and Vammala belts in Finland (e.g., Barnes et al., 2009), the Aguablanca deposit in the Variscan orogenic belt, Spain (e.g., Pina et al., 2010), the Selebi-Phikwe belt, Botswana (Maier et al., 2008), and the Savannah Ni-Cu-Co Camp, Australia (Le Vaillant et al., 2020). The Xiarihamu Ni-Co deposit in the East Kunlun Orogenic Belt (China) and the Nova Ni-Cu-Co deposit in the Albany-Fraser Orogenic Belt (Australia) have raised growing hopes of prospecting magmatic sulfide deposit in orogenic belts are the largest Ni deposit discoveries in the world since Voisey's Bay (Canada) (Li et al., 2015; Song et al., 2016; Maier et al., 2016 and references therein). However, the factors affecting metal grades of the sulfide ores have still not been well understood.

The E-W trending and ca.600-km-long Huangshan-Jingerquan metallogenic belt is the largest Ni-Cu sulfide metallogenic belt recognized in orogenic belts worldwide (Mao et al., 2008; Song et al., 2013, Song et al., 2021; Lightfoot and Evans-Lamswood, 2015). It is located in the North Tianshan in the southern margin of the Central Asian Orogenic Belt (CAOB) (e.g., Şengör et al., 1993; Xiao et al., 2013, Xiao et al., 2015). Since 1980′s, the Ni-Cu metallogenic belt has attracted great attentions as a number of economically large Ni-Cu sulfide deposits were

* Corresponding author at: State Key Laboratory of Ore Deposit Geochemistry, Institute of Geochemistry, Chinese Academy of Sciences, Guiyang 550081, PR China.
E-mail address: songxieyan@vip.gyig.ac.cn (X.-Y. Song).

https://doi.org/10.1016/j.oregeorev.2023.105465
Received 16 January 2023; Received in revised form 11 April 2023; Accepted 2 May 2023
Available online 9 May 2023

discovered, including Huangshan, Huangshandong, Huangshannan, Tudun, Xiangshan, Hulu and Tulaergen (Wang et al., 2006; Mao et al., 2008 and references therein) (Fig. 1). After 2000, several new discoveries along this belt were made by means of prospecting programs, such as the Tulaergen Ni-Cu deposit and the sulfide-mineralized Dahuangshan and Jingerquanbei mafic–ultramafic complexes (San et al., 2003; Song et al., 2021 and references therein). The Ni-Cu deposits along this metallogenic belt contain ~ 2.5*10^{8} tonnes sulfide ores with averaged Ni grade of 0.4–0.5 wt%, which is ~ 1/3 Ni metal reserves of all Ni-Cu sulfide deposits in the orogenic belts in China (Mao et al., 2008 and references therein). The genetically related basaltic magmatism was attributed to subduction (Zhang et al., 2011; Han et al., 2013), upwelling of asthenosphere due to break-off of subduction slab in syn- or post-collisional setting (Song et al., 2011, Song et al., 2013) and the Tarim mantle plume (Pirajno et al., 2008; Qin et al., 2011). Latest U-Pb dating of zircons separated from the sulfide-bearing rocks indicate that the sulfide mineralization occurred in a short period of 285 to 280 Ma, which is closely associated with high degrees partial melting of the asthenospheric mantle in early stage of post-collision, although the basaltic magmatism was prolonged from subduction (380–300 Ma) to post-collision (280–270 Ma) along the belt (Song et al., 2021). The sulfide ores from these deposits have a range of Se/S ratios (47 × 10^{-6}-420 × 10^{-6}) evidently larger than the mantle (Se/S = 230 × 10^{-6}-350 × 10^{-6}) and the country rocks (Se/S = 6.2 × 10^{-6}-115 × 10^{-6}). They have smaller range of δ^{34}S values (-0.9 to 1.4 ‰) relative to the country rocks of the deposit hosting mafic–ultramafic complexes (δ^{34}S = –22.3 to + 18.8‰). These phenomena demonstrated that sulfide liquid immiscibility occurred in deep levels in the crust, rather than *in-situ* (Deng et al., 2022). Along the magma plumbing systems, deposition of the sulfides at deep levels formed mineralized dykes and formed stratiform and lenticular shaped orebodies in large mafic–ultramafic complexes at shallow levels (Song et al., 2021; Deng et al., 2021).

Each of the Ni-Cu sulfide deposits along the Huangshan-Jingerquan metallogenic belt has been studied in the past ten years and a lot of Ni, Cu and platinum-group elements (PGE) data of the sulfide ores have been reported (Zhang et al., 2011; Gao et al., 2013; Deng et al., 2014,

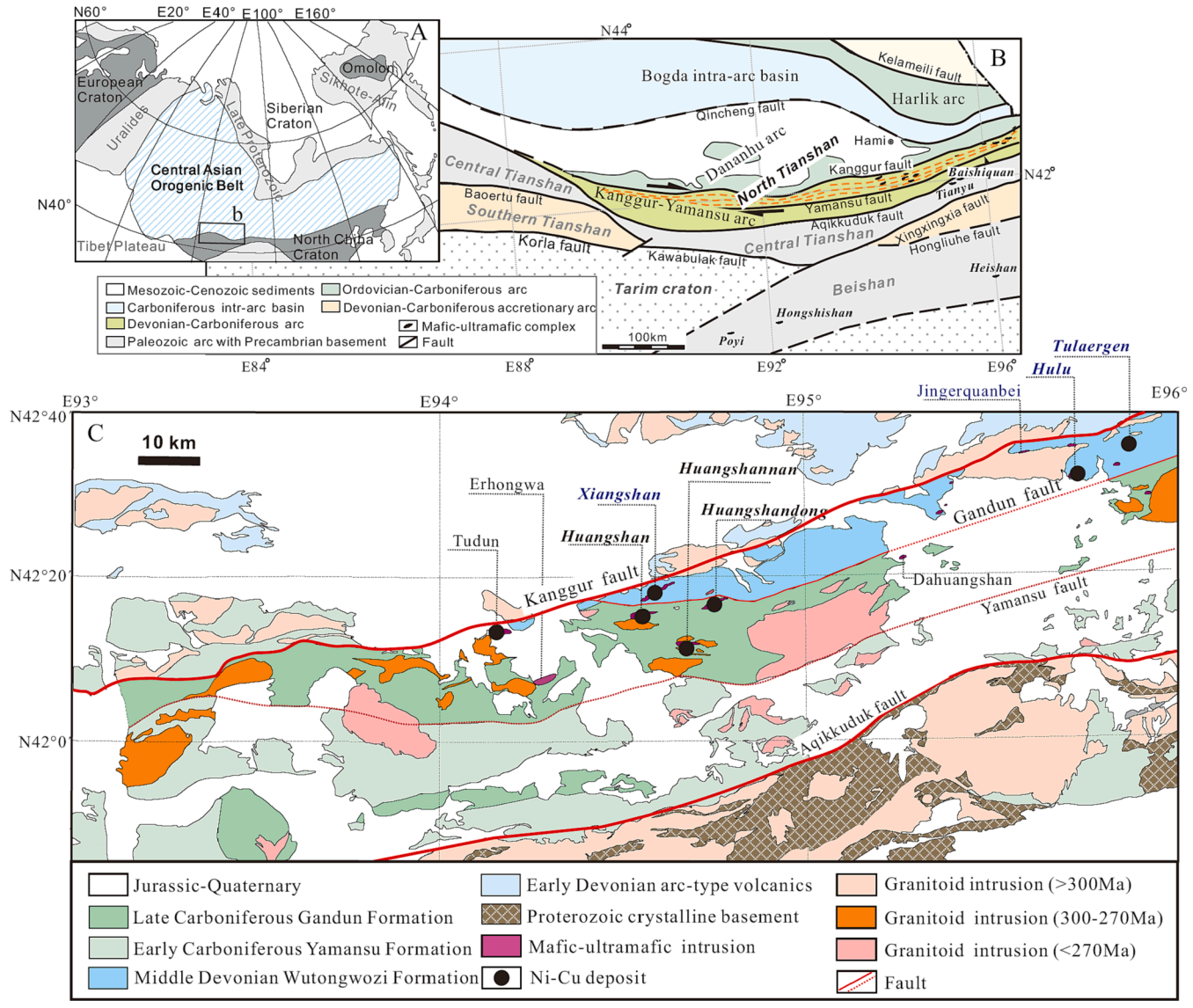

Fig. 1. A. Location of the Central Asian Orogenic Belt. B. The North Tianshan arc system is bounded by the Kelameili and Aqikkuduk faults and consists of the Harlik-Dananhu island arc in the north and the Kanggur-Yamansu arc in the south (after Xiao et al., 2013). C. Geological map of the Kanggur-Yamansu arc. The Huangshan-Jingerquan Ni-Cu metallogenic belt is located to the north of the Yamansu fault (after Song et al., 2013 and references therein). The mafic–ultramafic complexes are emplaced in Middle Devonian Wutongwozi Formation and Late Carboniferous Gandun Formation. Names of the complexes hosting large Ni-Cu sulfide deposits are bold italics.

Deng et al., 2017; Tang et al., 2014; Mao et al., 2014, Mao et al., 2015; Zhao et al., 2016; Wang et al., 2018; Zhao et al., 2018 and references therein). However, some issues important for better understanding magmatic sulfide mineralization along the metallogenic belt have not been addressed well: (1) chemical characteristics of the parental magmas, (2) mechanisms of sulfide migration and deposition in magma plumbing systems, (3) processes resulting in geochemical discrepancies and variations of the sulfide ores. In this study, the published Ni, Cu and PGE data of the sulfide ores of the main magmatic sulfide deposits and the sulfide-poor rocks from the hosting complexes are integrated to address the above issues. This study gives overall insights on conditions and processes of sulfide segregation, differentiation, migration and deposition in the metallogenic belt. These insights are significant for understanding of the formation of Ni-Cu sulfide deposits in orogenic belts.

2. Geological background

The ~ 5500-km-long CAOB is the largest Phanerozoic accretionary orogenic system in the world (Fig. 1A) (e.g., Şengör et al., 1993; Xiao et al., 2013, Xiao et al., 2015). It is situated among the eastern European Craton to the west, Siberian Craton to the northeast, and North China-Tarim Craton to the south. The Chinese East Tianshan is eastern portion of the east–west-trending Tianshan Mountain, which constructs the southern margin of the CAOB.

The Chinese East Tianshan can be further subdivided into North, Central and South Tianshan terranes by regional fault zones, respectively. A series of Ni-Cu sulfide deposits have been discovered along the Huangshan-Jingerquan belt in North Tianshan, Central Tianshan (Baishiquan, Tianyu, etc.) and Beishan Belt (Poyi, Heishan, etc.) (Mao et al., 2008; Chai et al., 2008; Xia et al., 2013; Xue et al., 2016; Xie et al., 2012, Xie et al., 2014; Song et al., 2021). Central Tianshan has a Precambrian basement, which is overlain by Paleozoic metamorphosed volcanic and sedimentary rocks and South Tianshan dominantly comprises of Devonian-Carboniferous accretionary complexes (e.g., Wang et al., 2014). North Tianshan between the Kelameili and Aqikkuduk faults is an arc system (Fig. 1B). Recognitions of ophiolites (417–330 Ma) along Aqikkuduk fault as well as radiolaria and conodonts in the Devonian to Carboniferous siliceous sediments demonstrate existence of the North Tianshan Ocean in Paleozoic in the Chinese East Tianshan (e.g., Xiao et al., 2013; Han and Zhao, 2018). The Kanggur fault divides the North Tianshan arc system into the Harlik-Dananhu island arc to the north and the Kanggur-Yamansu arc to the south (Fig. 1B). In the Harlik-Dananhu arc, Ordovician to Carboniferous calc-alkaline intermediate-acid intrusive and volcanic rocks were attributed to northward subduction of the North Tianshan Ocean (e.g., Chen et al., 2013). The Kanggur-Yamansu arc was regarded as an accretionary prism and a volcanic zone developed along the northern margin of the Central Tianshan block due to southward subduction of the North Tianshan Ocean (Chen et al., 2019).

3. The Ni-Cu sulfide deposits of the Huangshan-Jingerquan metallogenic belt

The Huangshan-Jingerquan Ni-Cu metallogenic belt is situated in northern portion of the Kanggur-Yamansu arc (Fig. 1, Chen et al., 2019). The southern dipping Gandun fault divides the metallogenic belt into the northern and southern parts (Fig. 1C). The northern part is occupied by the middle Devonian Wutongwozi Formation, which mainly consists of metasandstone with interlayers of tuff and marble. The southern part is occupied by the late Carboniferous Gandun Formation mainly consisting of siliceous slates and metasandstones with interlayers of marble (Deng et al., 2021).

3.1. Deposits hosted in the complexes within the Gandun Formation

The mafic–ultramafic complexes emplaced in the Gandun Formation have large scales, bean-pod, rhombic or oval outlines, and funnel shaped vertical cross sections. Stratiform and lenticular shaped Ni-Cu sulfide orebodies are mostly embedded in ultramafic facies (Song et al., 2021). Huangshandong and Huangshan are the two largest Ni-Cu sulfide deposits in the Huangshan-Jingerquan metallogenic belt and contain 0.33 and 0.38 million tonnes Ni metal, respectively (Appendix Table 3).

The Huangshandong complex is 3.5 km long and 1.2 km wide with a perfect rhombic outline (Fig. 2A). Its bottom extends to more than 1000 m deep in the west and becomes shallow to the east. The complex dominantly consists of gabbroic rocks and lherzolite occurs as interlays within or overlaying the ilmenite-bearing gabbro. Lithological relationships and sharp contacts among these lithofacies demonstrate emplacement of multiple pulses of basaltic magma (Fig. 2A, Gao et al., 2013; Deng et al., 2014 and references therein). Concave layered and lenticular disseminated Ni-Cu sulfide orebodies dominantly occur at the base of the lherzolite and within the gabbronorite, respectively (Fig. 2A).

The bean-pod shaped Huangshan complex is ~ 2.5 km long and shrinks to the east (Fig. 2B, Zhou et al., 2004). Funnel-shaped cross sections down to depths more than 1000 m suggested a magma feeder conduit on the west (Lightfoot and Evans-Lamswood, 2015). It mainly comprises lherzolite and websterite, which gradually change to gabbronorite and olivine gabbro upward. Lenticular disseminated Ni-Cu sulfide orebodies occur at the bases of the lherzolite and websterite (Fig. 2B). Intermittent emplacement of multiple pulses of magma is indicated by sharp contacts between the lherzolite and underlying basal gabbronorite (Deng et al., 2015, Deng et al., 2017 and references therein). Additionally, fine-grained lherzolite overlays gabbronorite at the surface in central part of the complex (Fig. 2B). This is confirmed by distinguishable zircon U-Pb ages of different lithologies (Fig. 2B, Song et al., 2021).

The Huangshannan complex is similar to the Huangshandong complex in shape, size and rock types, but have much smaller proportions of ultramafic rocks, which contain a few economic Ni-Cu orebodies (Fig. 2C, Mao et al., 2017). The small oval shape Tudun complex has high proportion of lherzolite and hosts economic Ni-Cu orebodies (Appendix Table 3, Fig. 2D, Song et al., 2013; Wang et al., 2015).

3.2. Deposits hosted in the complexes within the Wutongwozi Formation

Most of the mafic–ultramafic complexes emplaced in the Wutongwozi Formation appear as dykes or chains of small pods with exception of the Hulu complex. Some of them hosted small economic Ni-Cu sulfide deposits (Appendix Table 3) (Song et al., 2021).

The Tulaergen complex is a ~ 800 m long mafic–ultramafic dyke and hosts the third largest Ni-Cu sulfide deposit (~0.12 million tonnes Ni metal, Appendix Table 3) in the Huangshan-Jingerquan metallogenic belt. It consists of lherzolite, websterite and gabbro from the center to the margin and several lenticular shaped Ni-Cu sulfide orebodies occur within the lherzolite (Jiao et al., 2013; Wang et al., 2018 and references therein) (Fig. 2E, Appendix Table 3). The Xiangshan complex is a ~ 8 km long olivine gabbro dyke with widths up to 1 km. Several disseminated Ni-Cu sulfides mineralized lherzolite bodies (up to 1 km long and 300 m wide) are enveloped by the olivine gabbro (Shi et al., 2018 and references therein) (Fig. 2F, Appendix Table 3). The Hulu complex is ~ 2 km long and up to 1 km wide and has a lopolith outline shrinking in the middle (Han et al., 2013). In the complex, lherzolite is underlain by harzburgite and websterite constructs the bottom in the western portion. Ni-Cu sulfide ore layers mainly lie in the basal websterite (Fig. 2G, Appendix Table 3). Olivine-free gabbro occurs along the complex margins (Zhao et al., 2018).

Other complexes emplace in the Wutongwozi Formation appear as chains of small ultramafic bodies containing sparsely disseminated

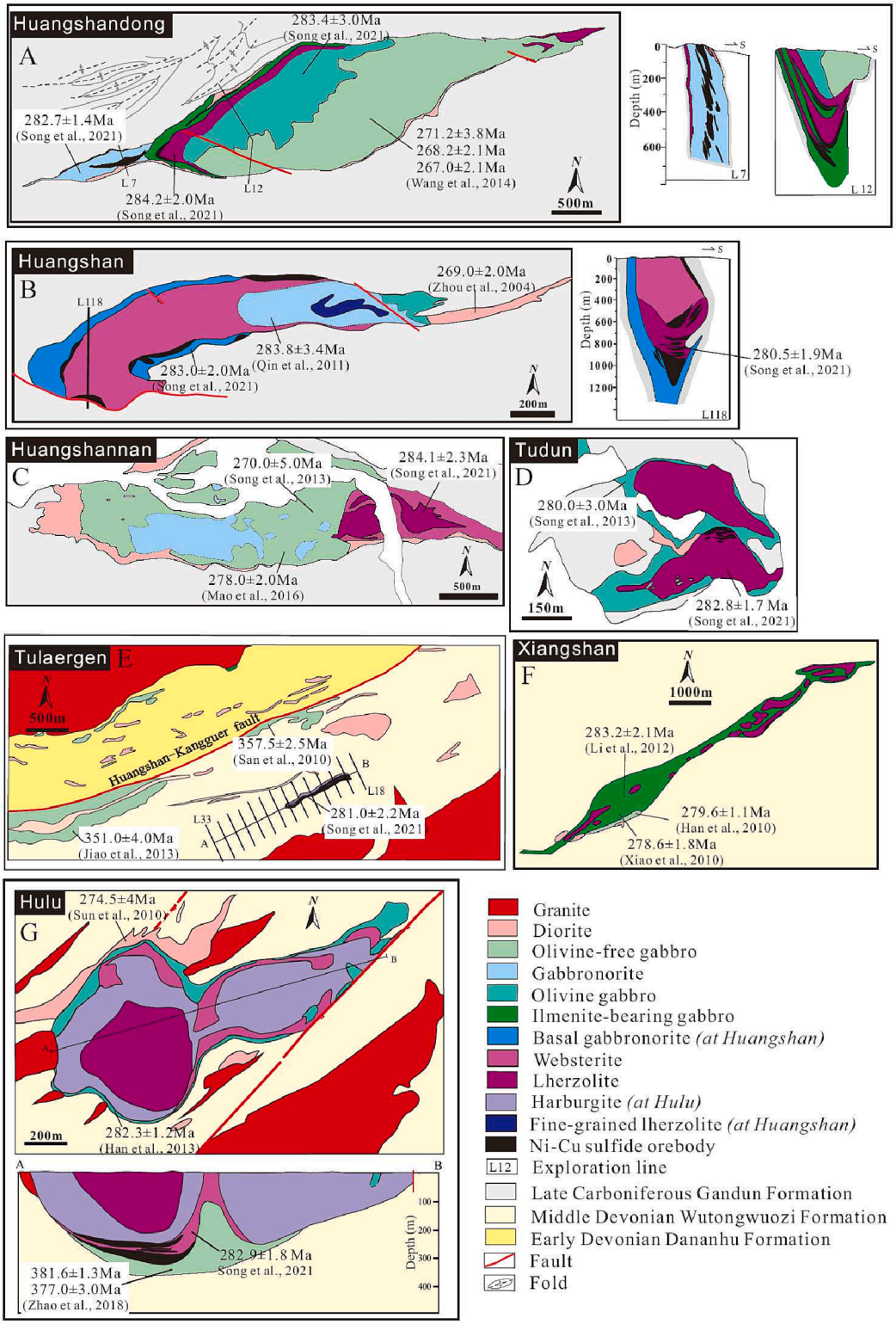

Fig. 2. Simplified geological maps of the mafic–ultramafic complexes hosting large Ni-Cu sulfide deposits along the Huangsha-Jingerquan metallogenic belt (after Song et al., 2021 and references therein). The complexes emplaced in the Gandun Formation are large and have rhombic or oval outlines, such as Huangshandong (A), Huangshan (B), Huangshannan (C), Tudun (D). The complexes emplaced in the Wutongwozi Formation appear as dykes or chains of small pods, such as Tulaergen (E) and Xiangshan (F), exception for the Hulu sill (G). Locations of the complexes are shown in Fig. 1C.

sulfides. For instance, the Chuanzhu complex is a ~ 1.6 km long chain including a series of small ultramafic outcrops containing disseminated sulfides in Gobi desert (Appendix Table 3).

4. Ni, Cu and PGE concentrations of sulfide-poor rocks

The sulfide-poor mafic and ultramafic rocks from the major complexes along the Huangshan-Jingerquan metallogenic belt commonly contain minute amount of sulfides with whole-rock sulfur<0.2 wt% (Sun et al., 2013; Mao et al., 2014, Mao et al., 2015; Wang et al., 2015). The sulfides (mainly pyrrhotite, pentlandite and chalcopyrite) are interstitial among silicates in the sulfide-poor rocks (Appendix Fig. 1). The sulfide-poor rocks display positive correlations between Ir and the other PGEs due to existences of the sulfides (Fig. 3A-C). In spite of this, their PGE concentrations (<0.12 ppb Ir, <0.15 ppb Ru, 0.1–3.0 ppb Pt (except for one point) and 0.13–2.3 ppb Pd, Appendix Table 1) are evidently lower

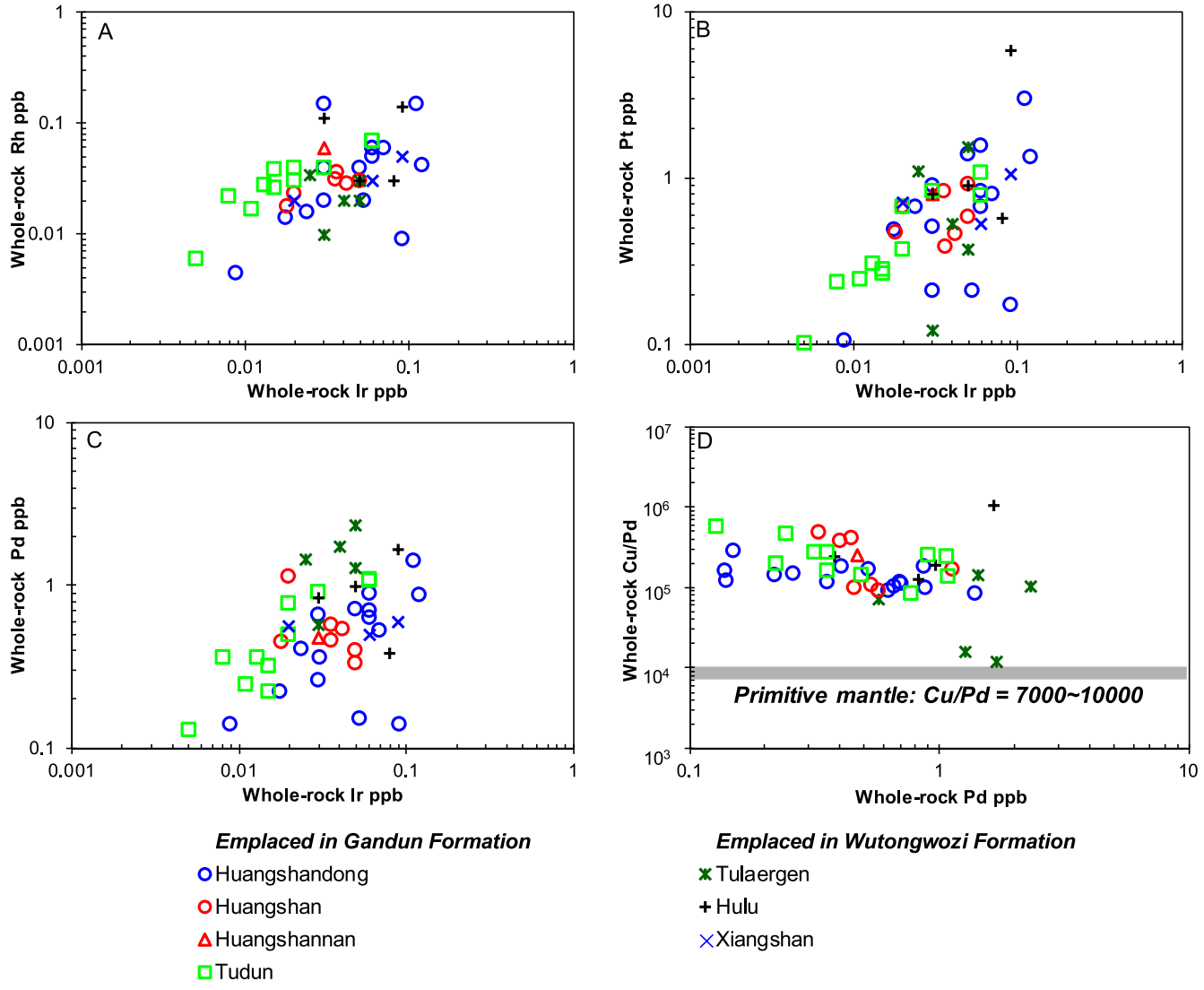

Fig. 3. Binary diagrams of Ir versus Rh (A), Pt (B), Pd (C) and Cu/Pd (D) for the sulfide-poor mafic–ultramafic rocks from the Huangshan-Jingerquan complexes (Tang et al. 2014; Deng et al. 2014, 2015; Mao et al. 2016, 2017; Wang et al. 2018 and references therein). Data are listed in Appendix Table 1. Estimated Cu/Pd value of the primitive mantle (7000 ~ 10000) is from Barnes and Maier (1999).

than those of S-undersaturated oceanic island basalts from Iceland, which contain 7.58 ± 0.3 ppb Pd and 0.189 ± 0.005 ppb Ir (Rehkämper et al., 1999). In addition, Cu/Pd values of the sulfide-poor rocks are evidently higher than those of the primitive mantle (7000–10000, Barnes and Maier, 1999) (Fig. 3D). Analytical methods of sulfur and PGE are summarized in Supplementary information.

5. Ni, Cu and PGE concentrations of sulfide ores

The Ni-Cu sulfide ores from the deposits in the Huangshan-Jingerquan metallogenic belt are classified into three groups according to sulfur contents (Appendix Table 2): disseminated ore (S < 3.0 wt %), densely disseminated ore (S = 3.0–10.0 wt%) and net-textured/massive ores (S greater than 10.0 wt%) (Appendix Fig. 2), for convenience in description and discussion below. As shown in Fig. 4A, B, the disseminated and densely disseminated ores have positive correlations between S contents and grades of Ni and Cu, while the net-textured/massive ores display large variation in Cu grades at given S contents. The sulfide ores from most of the deposits display positive correlations between S and PGE, whereas the sulfide ores from the Tulaergen deposit display the largest variation in PGEs (Fig. 4C-E).

In binary diagrams in bases of 100% sulfide (express using subscript $_{[100]}$), most of the sulfide ores clearly show positive correlations of $Ru_{[100]}$ and $Rh_{[100]}$ against $Ir_{[100]}$, but large variations in $Pt_{[100]}$ and $Pd_{[100]}$ (Fig. 5A-D). It is worth to note that the disseminated ores show good positive correlations between $Ir_{[100]}$ and the other PGEs and plotted in narrow areas circled by light blue dashed lines in Fig. 5A-D. In contrast, the densely disseminated and net-textured/massive ores plot dispersedly in the diagrams of $Pt_{[100]}$ and $Pd_{[100]}$ against $Ir_{[100]}$ owing to large variation of $Pt_{[100]}$ and $Pd_{[100]}$ in given $Ir_{[100]}$ (Fig. 5C-D). The sulfide ores from the Huangshan deposit are featured by high Ru/Ir values and small ranges of Pt/Ir and Pd/Ir values relative to those from other deposits (Fig. 5A, C, D). Conversely, the Huangshandong and Huangshannan sulfides are marked by the large variations in the ratios of Pt/Ir and Pd/Ir (Fig. 5C, D). Those from the Huangshannan deposit are characterized by relatively high Ni, Ir, Ru and Rh tenors (Fig. 5, Mao et al., 2017). Comparing with other deposits, the Tulaergen sulfide ores display remarkably large variations in tenors of these metals, particularly, the Cu-rich massive ores are not only characterized by low Ni/Cu values but also extremely large variation in $Pt_{[100]}$ (Fig. 5). Their highest Ru/Ir and Rh/Ir ratios of the Cu-rich massive ores are resulted from interferences of high Cu content in analyses and not significant in geochemistry (see Supplementary information).

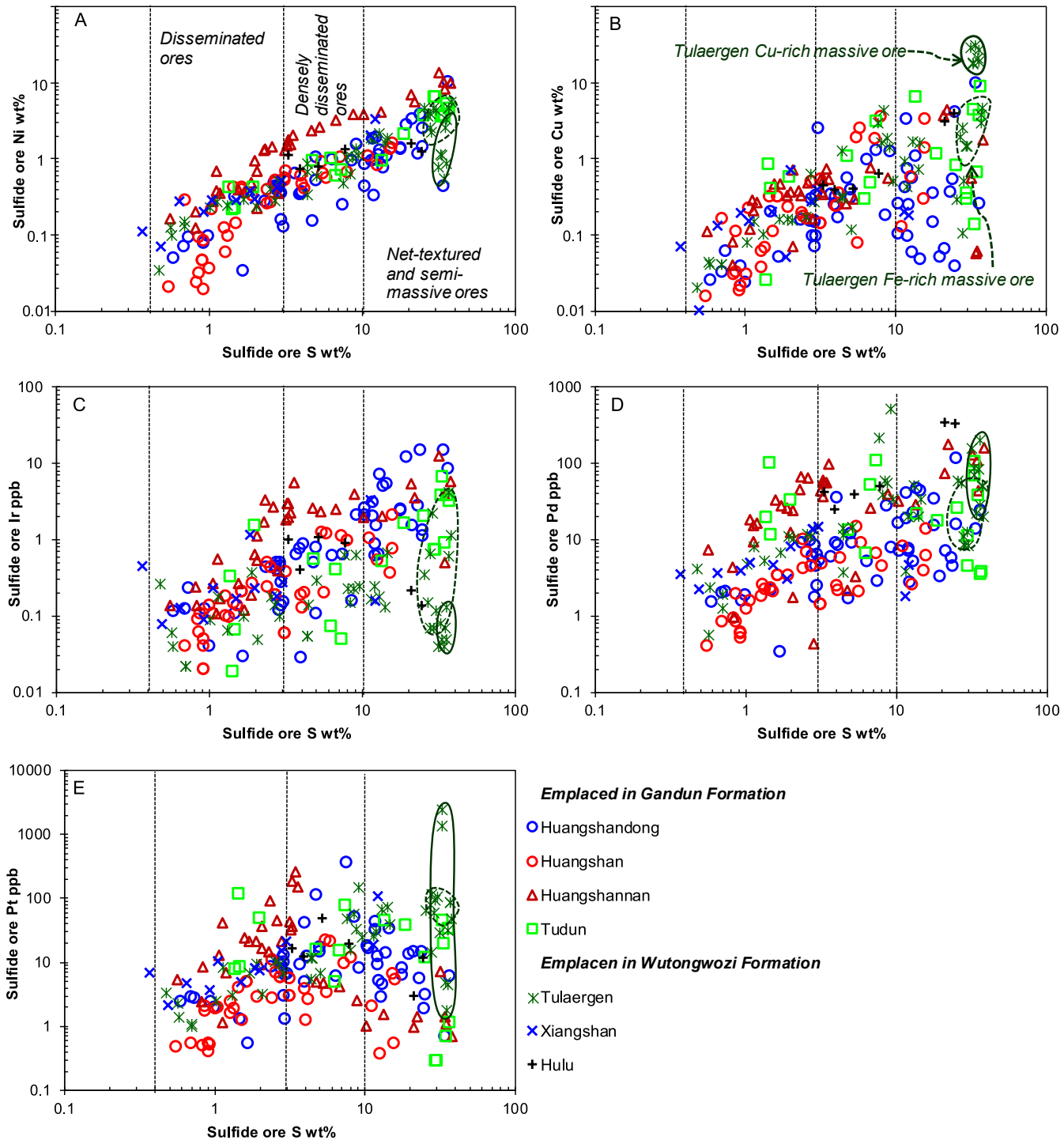

Fig. 4. Binary plots of sulfur versus contents of Ni (A), Cu (B), Ir (C), Pd (D) and Pt (E) of the sulfide ores from the Ni-Cu sulfide deposits along the Huangshan-Jingerquan metallogenic belt. Data are from Appendix Table 1.

6. Discussion

6.1. PGE-depleted parental/primary magmas

Nickel and Cr are compatible but Cu and Y are incompatible for olivine and pyroxenes (Kelemen, 1990). Chromium is a major element of chromite. The sulfide-poor rocks contain<1.0 modal% chromite, which was commonly crystalized together with or slightly later than olivine. Therefore, Ni and Cr could be enriched in cumulus of mafic minerals and Cu and Y are remained in residual magmas during fractionation before sulfide/silicate liquid immiscibility occurs. On the other hand, both Ni and Cu tend to be concentrated in sulfide liquid if sulfide/silicate liquid immiscibility occurs due to their high sulfide liquid/silicate melt partition coefficients, while Cr and Y are incompatible for sulfide liquid (Fleet et al., 1999a; Fleet et al., 1999b; Mungall and Brenan, 2014). The negative correlation of Cr against Y of the sulfide-poor mafic–ultramafic rocks indicates accumulation of olivine and pyroxenes (Fig. 6A). However, the positive correlations of Ni and Cu against Cr manifest the sulfide-poor rocks containing minute amount of sulfides (Fig. 6B, C). Copper is strongly concentrated in sulfide liquid as a chalcophile

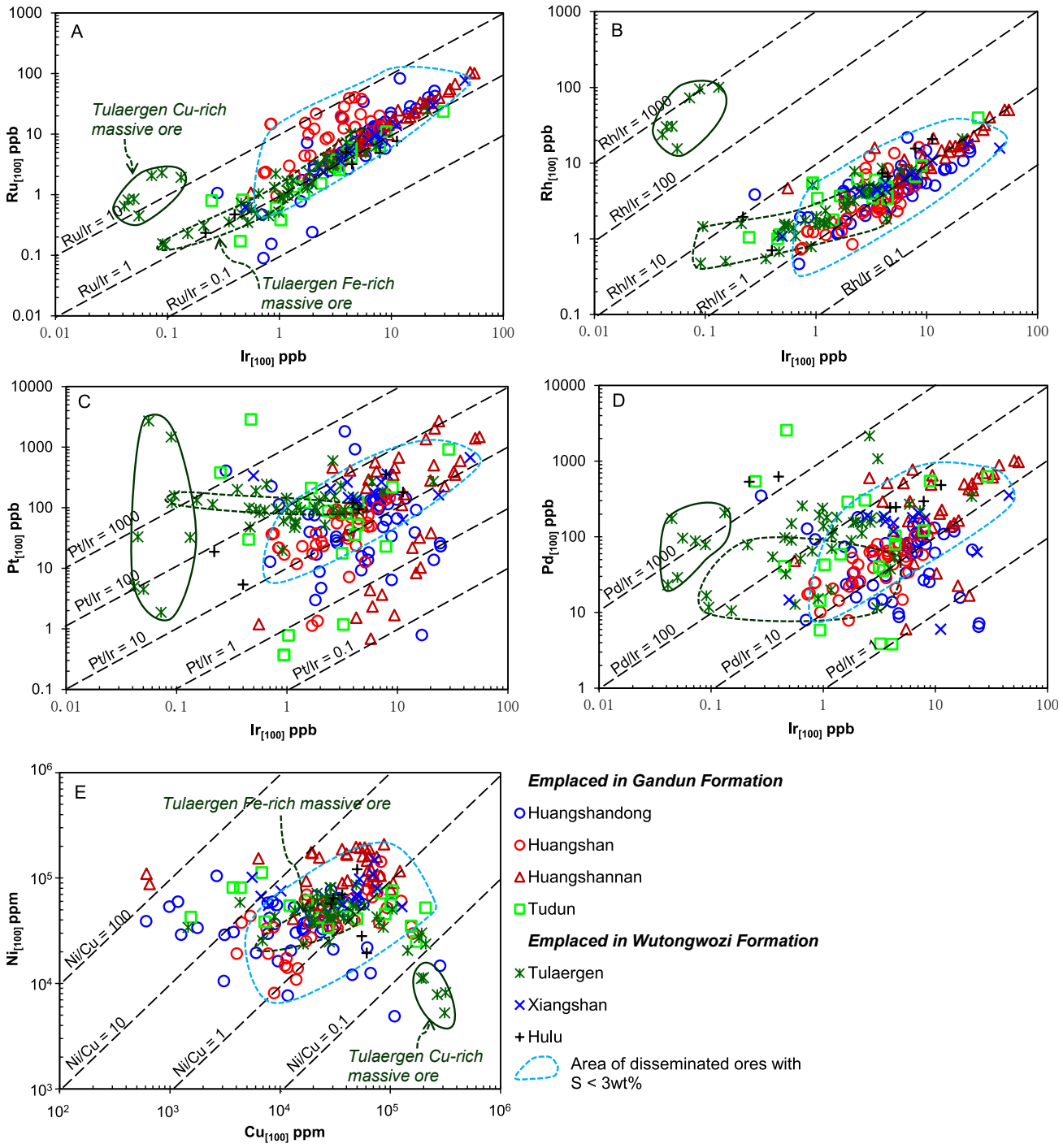

Fig. 5. Binary plots of Ir versus Ru (A), Rh (B), Pt (C) and Pd (D) and Cu versus Ni (E) for the sulfide ores in 100% sulfide basis for the Ni-Cu sulfide deposits along the Huangshan-Jingerquan metallogenic belt. The unusually high $Rh_{[100]}$ and $Ru_{[100]}$ and extremely high Ru/Ir and Rh/Ir values of the Tulaergen Cu-rich massive ores are the results of interferences of the high Cu content and not significant in geochemistry (see Supplementary material). Data are after Appendix Table 1.

element and Y is remained in silicate melt as a lithophile element when sulfide-silicate liquid immiscibility occurs (Lightfoot et al., 1997; Song et al., 2009a). Therefore, positive correlations of Pt and Pd against Cu/Y testify that PGE are dominantly concentrated in the minute amounts of sulfides (Fig. 6D, E). Thus, although the sulfide-poor rocks contain up to 2.3 ppb Pd and 3.0 ppb Pt, their parental magmas should contain much lower Pd and Ir. Previous studies proposed that middle ocean ridge basalts (MORB) are variably depleted in PGE, containing up to 6.1 ppb Pd and 2.5 ppb Pt, respectively, owing to sulfide retention in the mantle source under low degrees partial melting (Rehkämper et al., 1999). Therefore, it is reasonable to consider that the parental magmas of the sulfide-poor rocks are PGE-depleted (Zhang et al., 2011; Deng et al., 2014; Deng et al., 2017; Tang et al., 2014; Zhao et al., 2015). This is supported by that all of the sulfide-poor rocks have Cu/Pd values much higher than that of primitive mantle (Cu/Pd $\leq 10^4$, Barnes and Maier, 1999) (Fig. 3D).

6.2. *Quantitative approach to PGE-depletion of parental magma*

Compositional variations of magmatic sulfides are controlled by the

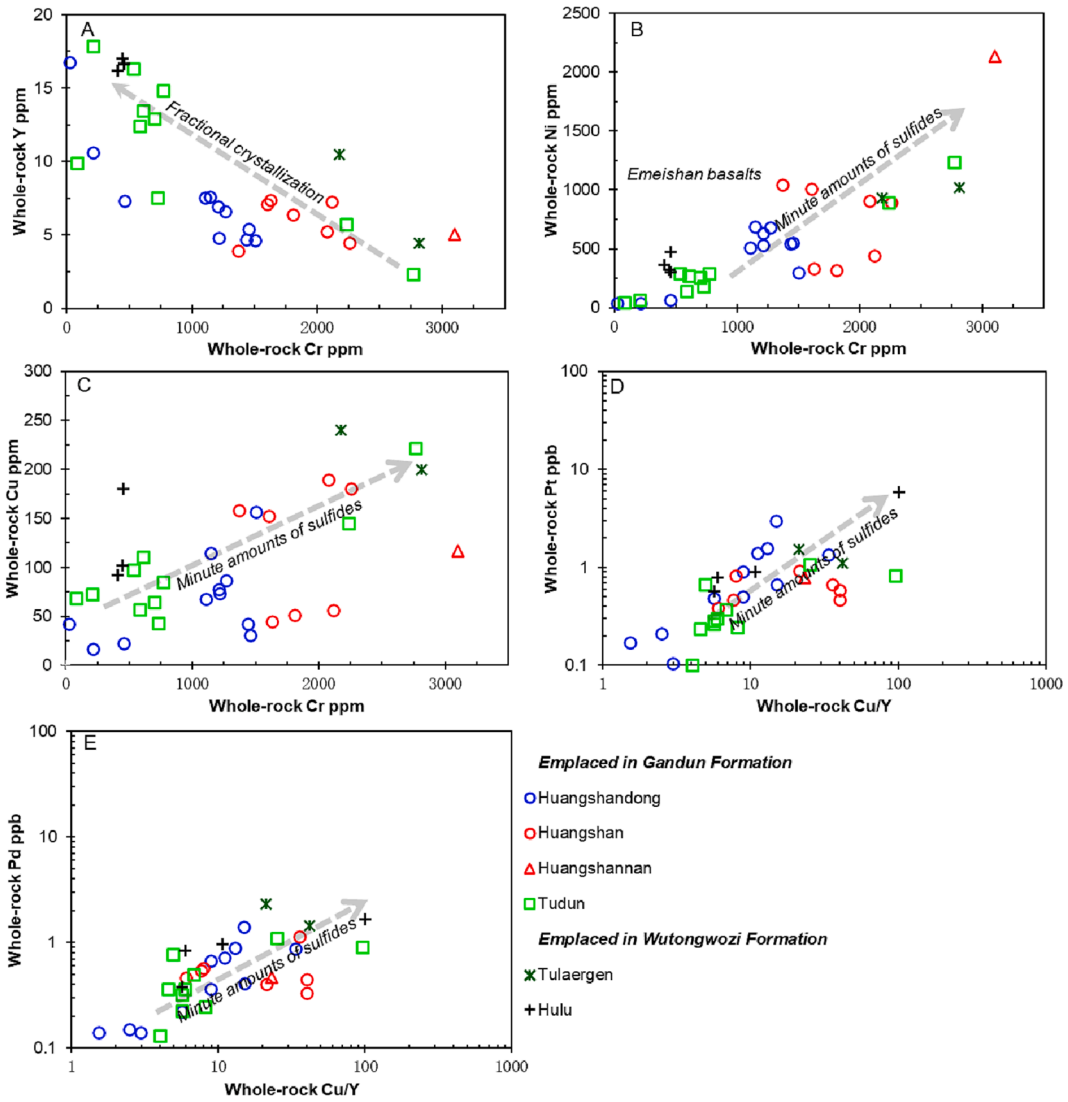

Fig. 6. Binary plots of Cr versus Y (A), Ni (B) and Cu (C), Y versus Cu (D), Cu/Y versus Pt (E) and Pd (F) for the sulfide-poor mafic–ultramafic rocks for the Huangsha-Jingerquan complexes. Data are from Appendix Table 2.

processes including sulfide segregation from basaltic magma, fractionation of the sulfide liquid, mixture of the sulfide liquids and reaction of the sulfides with recharged magma. Abundances of PGE of basaltic magma prior to sulfide/silicate liquid immiscibility are associated with degree of partial melting and fractional crystallization (see below). Because sulfide liquid/silicate melt partition coefficients of PGEs are quite similar to each other, differentiation between PGEs during sulfide segregation is commonly negligible (Mungall and Brenan, 2014). In contrast, fractional crystallization of monosulfide solid solution (MSS) can lead to residual liquid gradually enriched in Pt and Pd and depleted in Ir and Ru, because Ir and Ru are compatible to MSS but Pt and Pd are incompatible (Liu and Brenan, 2015). Positive correlations of $Ir_{[100]}$ against tenors of other PGE indicate limited differentiation among PGE for the disseminated ores with S < 3 wt% shown by the blue dashed circles (Fig. 5A-D). Thus, the disseminated ores could better represent the compositions of the sulfide liquids initially segregated from the parental magmas. Equation proposed by Campbell and Naldrett (1979) is employed to model sulfide segregation of the disseminated sulfides:

$$C_S = C_l{}^*D^*(R+1)/(R+D) \quad (1)$$

C_S and C_l mean concentrations of an element in sulfide liquid and silicate melt, respectively, D is sulfide liquid/silicate melt partition coefficient of that element; R is mass ratio between silicate melt and sulfide liquid. In the calculation, $D_{Pd}^{Sul/Sil}$, and $D_{Cu}^{Sul/Sil}$ are assumed to be $3*10^6$ and 10^3, respectively (Mungall and Brenan, 2014). Recent studies of whole-rock and mineral geochemistry of the mafic–ultramafic complexes in the Huangshan-Jingerquan metallogenic belt proposed that the basaltic magmas were derived from partial melting of the upwelling asthenosphere and adjacent metasomatized mantle in early-stage of post-collision (Song et al., 2013, Song et al., 2021). Thus, it is assumed that the parental magma was compositionally similar to MORB, which is common PGE-depleted and contains 0.46 ppb Pd and 88 ppm Cu (Crockett, 2002; Rehkämper et al., 1999). Calculation according to the equation (1) indicates that most of the disseminated ores are plotted below the model trend of the sulfide liquids segregated from MORB-like magma (Fig. 7). Thus, a more PGE-depleted magma containing 0.023 ppb Pd and 79 ppm Cu may be another end member of parental magma from which the sulfide liquids segregated. This indicates that the initial sulfides of the deposits in the Huangshan-Jingerquan metallogenic belt were segregated from variably PGE-depleted magmas under R factor values ranging from 100 to 2000, even for a single deposit.

Extraction of sulfides could leave the sulfides behind in feeder system or staging chamber and cause intense PGE-depletion in the ascending basaltic magma (Song and Li, 2009; Chen et al., 2013). It was proposed that variable PGE-depletion of the parental magma of the mafic–ultramafic complexes in the Huangshan-Jingerquan metallogenic

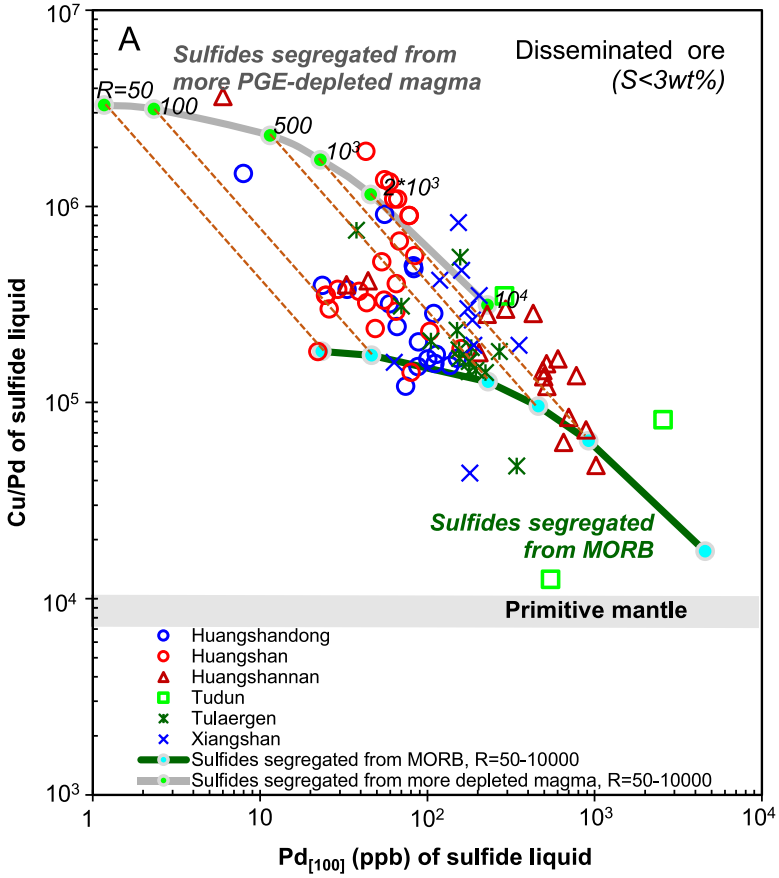

Fig. 7. Modeling of sulfide liquid segregation from variably PGE depleted basaltic magmas. The parental magmas were assumed to be PGE moderately depleted similar to MORB containing 0.46 ppb Pd and 88 ppm Cu (Crockett, 2002) and more PGE depleted magma containing 0.023 ppb Pd and 79 ppm Cu, respectively. In the calculations, $D_{Pd}^{sul/sil}$ and $D_{Cu}^{sul/sil}$ are assumed to be $3*10^6$ and 1000, respectively (Mungall and Brenan, 2014).

belt was resulted from prior sulfide removal (Zhang et al., 2011; Deng et al., 2014; Deng et al., 2017; Tang et al., 2014; Zhao et al., 2015). However, the disseminated sulfide ores from all of the deposits are PGE-depleted and have Cu/Pd values much larger than the primitive mantle (Fig. 7), even though reaction with basaltic magmas could result in elevation of $Pd_{[100]}$ and decrease of Cu/Pd values of some disseminated sulfides (see below). If more PGE-depleted basaltic magma containing 0.023 ppb Pd and 79 ppm Cu were produced by prior sulfide removal from a MORB-like magma containing 0.46 ppb Pd and 88 ppm Cu (Fig. 7) (Crockett, 2002), only ~ 0.001% sulfide was removed because sulfide liquid/silicate melt partition coefficients of PGEs are as high as 10^5-10^6 (Mungall and Brenan, 2014). However, such small amounts of sulfide liquid should be in extremely dispersed tiny droplets and therefore very difficult to overcome viscous resistance of the basaltic magma and remove from the magma completely (Robertson et al., 2016). Thus, it is more likely that the primary magma was sulfide saturated due to sulfide retention in the mantle at low degrees of partial melting (Keays, 1995; Arndt et al., 2005). On the other hand, recent studies on variable Ni-Cu-PGE sulfide mineralization in the post-subduction mafic–ultramafic complexes in the Ivrea Zone (Alps of Italy) indicated that sulfide supersaturation without external sulfur could result in sulfide segregation in the lower continental crust (Fiorentini et al., 2018; Holwell et al., 2019; Chong et al., 2021). Addition of SiO_2 and dilution of FeO in the mafic magma due to contamination of sulfide-poor crustal rocks could lead weak sulfide segregation (Zhang et al., 2009a, Zhang et al., 2009b). This raises a possibility that the pre-existing sulfides in staging magma chamber could absorb PGE from passing basaltic magmas. Such process probably could also accountable for more intense PGE-depletion of the parental magmas in the Huangshan-Jingerquan metallogenic belt. Based on comparability of depletions of Pt and Pd relative to primitive mantle between sulfide ores and MORB or island-arc basalts, Barnes et al. (2022) proposed that PGE depletion of the Nova-Bollinger Ni-Cu deposit in the Albany-Fraser orogeny, western Australia, was attributed to sulfide retention in the mantle during partial melting.

6.3. *Differentiation and upgrading of the sulfide liquids*

MSS/sulfide liquid partition coefficients of PGEs indicate that fractional crystallization of sulfide melt can result in differentiation between IPGE (Os, Ir, Ru) and PPGE (Pt and Pt) as well as between Ni and Cu in the sulfide cumulates and residual sulfide liquids (Fleet et al., 1993, Fleet et al., 1999a; Fleet et al., 1999b; Liu and Brenan, 2015). Moreover, the residual sulfide liquids rich in Pt and Pd may migrate above temperature of 1000℃ and resulting in heterogeneity of PGE in the ores (Holwell et al., 2022). For the sulfide ores of the deposits in the Huangshan-Jingerquan metallogenic belt, Pt is more variable than Pd (Fig. 5C, D), Pd/Ir ratio is therefore employed to illustrate the differentiation of sulfides. As shown in Fig. 8A and B, the sulfide ores show negative correlations between $Ir_{[100]}$ and Pd/Ir and positive correlation between $Pd_{[100]}$ and Pd/Ir. This is corresponding to differentiation between IPGE and PPGE carried out by fractional crystallization of MSS. Larger variations in PGE tenors and Pd/Ir values of the densely disseminated and net-textured/massive sulfide ores than the disseminated ores indicate that the former experienced more significant fractionation of MSS than the later (Fig. 8). Extremely high Pd/Ir values

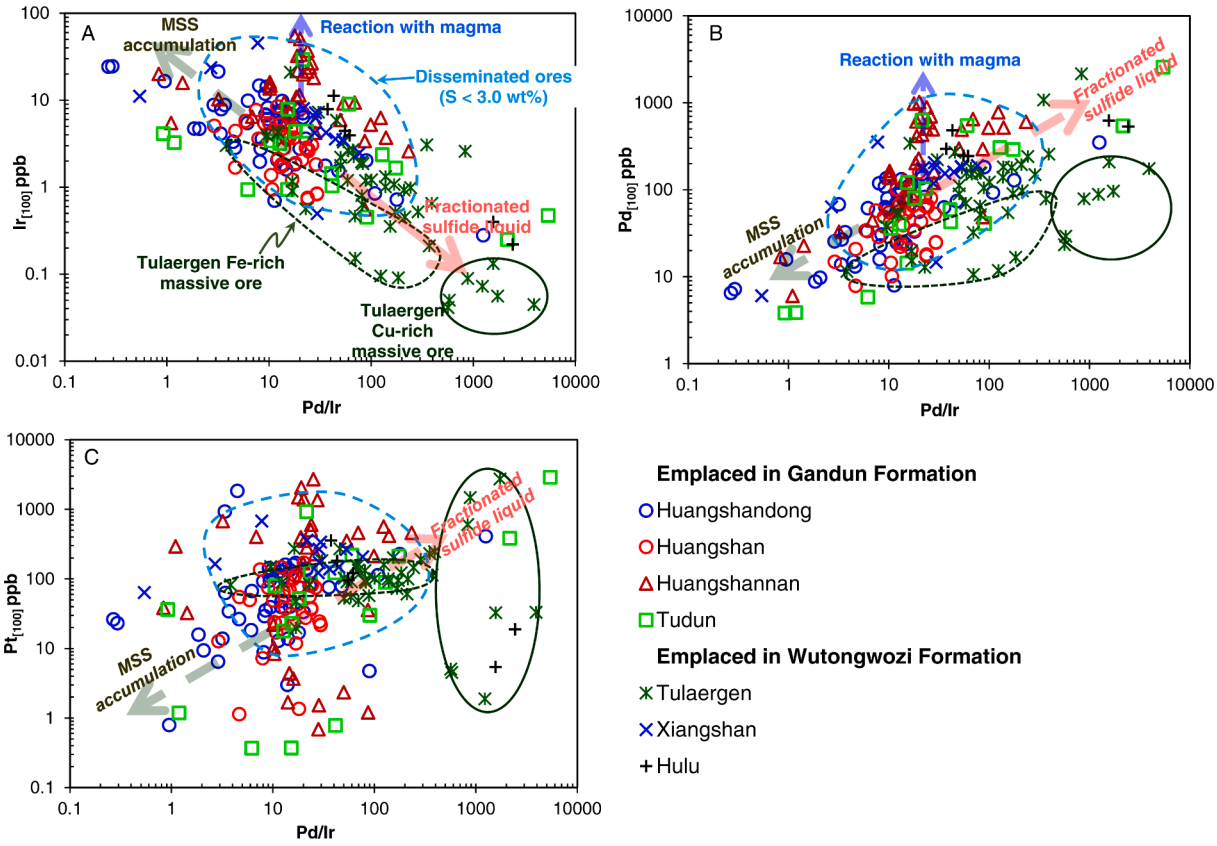

Fig. 8. Binary diagrams of Pd/Ir against $Ir_{[100]}$ (A), $Pd_{[100]}$ (B), and $Pt_{[100]}$ (C) for the sulfide ores from the Ni-Cu sulfide deposits along the Huangshan-Jingerquan metallogenic belt. Data are after Appendix Table 1.

demonstrate that the Tulaergen Cu-rich massive ore is solidification of differentiated sulfide liquid. Whereas, the Fe-rich massive ores plotted on the trends showing fractionation of sulfide liquid in the diagram of $Ir_{[100]}$ and $Pd_{[100]}$ versus Pd/Ir (Fig. 8A, B), indicating that the compositions of the Fe-rich massive ores are dominantly controlled by fractionation of the sulfide liquid.

However, large variations in $Ir_{[100]}$ and $Pd_{[100]}$ of the disseminated sulfide ores at given Pd/Ir values cannot be attributed to fractionation of MSS and implies some other factors played roles on compositional variation of the sulfides (Fig. 8A, B). IPGE and Pt are variably compatible for chromite, olivine and pyroxenes and Pd are completely incompatible (Puchtel and Humayun, 2001; Righter et al., 2004; Ely and Neal, 2002; Hill et al., 2000). Therefore, variable degree of fractional crystallization of mafic minerals could result in variations of PGE abundances and Pd/Ir values in the parental magmas before sulfide/silicate liquid immiscibility occurred (Fleet et al., 1999a; Fleet et al., 1999b; Mungall and Brenan, 2014; Song et al., 2009b). Forsterite percentages of the olivine in the Huangshan-Jingerquan complexes are mostly lower than 86%, indicating the parental magmas experienced fractional crystallization of mafic minerals before sulfide segregation (Deng et al., 2012, Deng et al., 2017; Liu et al., 2012; Jiang et al., 2014; Mao et al., 2014, Mao et al., 2015). Thus, fractional crystallization of olivine, pyroxene and chromite could give rise to variations in PGE abundances and Pd/Ir values of the parental magma. The sulfide liquids segregated from such parental magma would have initially variable PGE compositions prior to fractional crystallization of MSS.

On the other hand, concentrations of Ni, Cu and PGEs in the sulfide liquid can be elevated via reaction with basaltic magma (Song et al., 2008). The large ranges of $PGE_{[100]}$ of the sulfides at a given Pd/Ir value are also related to reaction with basaltic magma (Fig. 8A-C). Particularly, the evidently large variation of $PGE_{[100]}$ of the Huangshannan sulfides at Pd/Ir values of 10 to 20 can be better ascribed to metal upgrading via reaction with following batches of basaltic magmas without prior sulfide segregation. However, it could not be ruled out that the parental magmas of the Huangshannan deposit were less PGE depleted than those of other deposits.

6.4. *Mixing and remobilization of sulfide liquids in magma plumbing system*

Fig. 9 shows the calculations for PGE differentiation resulted from fractional crystallization of the densely disseminated and the net-textured/massive ores. In the calculations, MSS was assumed to be the only solid phase and $D_{Ir}^{MSS/sul}$, $D_{Pd}^{MSS/sul}$, $D_{Ni}^{MSS/sul}$ are 10, 0.13, and 0.5, respectively (Barnes et al., 1997). It was assumed that the initial sulfide liquid 1 is segregated from MORB-like magma, which contains 0.46 ppb Pd, 0.03 ppb Ir and 144 ppm Ni, respectively (Crockett, 2002), under R value of 1000 and contains 460 ppb Pd, 30 ppb Ir and 6.4 wt% Ni, respectively. The initial sulfide liquid 2 is assumed to be segregated from basaltic magma more depleted in PGE, which contains 0.023 ppb Pd, 0.001 ppb Ir and 143.3 ppm Ni, respectively (see above), and contains 20 ppb Pd, 1.0 ppb Ir and 6.34 wt% Ni under R value of 1000, respectively. The compositions of MSS cumulate and residual liquid for the sulfide liquid 1 and 2 were calculated according to the equations for Rayleigh fractionation model:

$$C_R/C_o = DF^{(D-1)} \quad (2)$$

$$C_l/C_o = F^{(D-1)} \quad (3)$$

where C_o, C_R, C_l are concentration of an element in initial sulfide liquid, MSS cumulate and corresponding residual liquid, respectively; D is MSS/sulfide liquid partition coefficient of the element; F is the proportion of fractionated MSS. In the calculations, F was assumed to be 0.01,

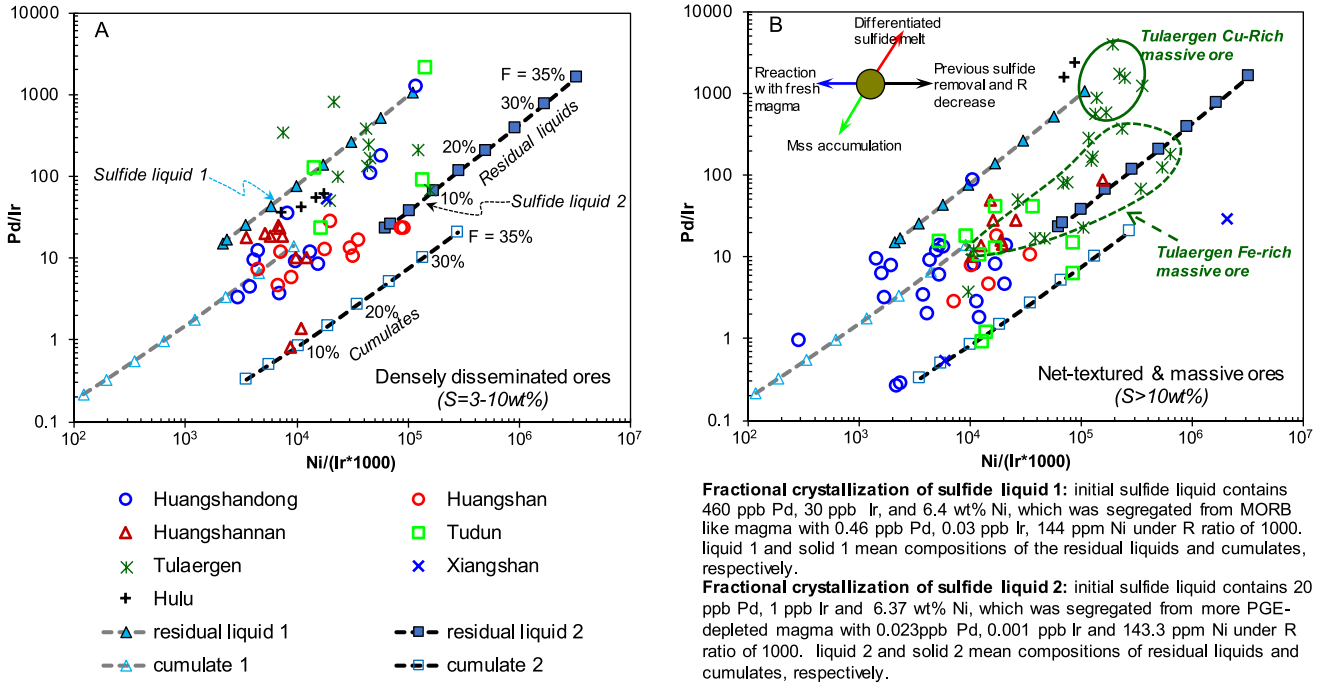

Fractional crystallization of sulfide liquid 1: initial sulfide liquid contains 460 ppb Pd, 30 ppb Ir, and 6.4 wt% Ni, which was segregated from MORB like magma with 0.46 ppb Pd, 0.03 ppb Ir, 144 ppm Ni under R ratio of 1000. liquid 1 and solid 1 mean compositions of the residual liquids and cumulates, respectively.

Fractional crystallization of sulfide liquid 2: initial sulfide liquid contains 20 ppb Pd, 1 ppb Ir and 6.37 wt% Ni, which was segregated from more PGE-depleted magma with 0.023ppb Pd, 0.001 ppb Ir and 143.3 ppm Ni under R ratio of 1000. liquid 2 and solid 2 mean compositions of residual liquids and cumulates, respectively.

Fig. 9. Modeling of differentiation of sulfide liquid of the densely disseminated ores (A) and net-textured and massive ores (B). In the calculations, monosulfide solid solution (MSS) was assumed to be the only solid phase. $D_{Ir}^{MSS/sul}$, $D_{Pd}^{MSS/sul}$, $D_{Ni}^{MSS/sul}$ (partition coefficient between MSS and sulfide liquid) are assumed to be 10, 0.13, and 0.5, respectively (Barnes et al., 1997). The initial sulfide liquid 1 was segregated from MORB like magma, which contains 0.46 ppb Pd, 0.03 ppb Ir and 144 ppm Ni, with silicate melt/sulfide liquid ratio of 1000. The initial sulfide liquid 2 was segregated from more PGE depleted basaltic magma, which contains 0.023 ppb Pd, 0.001 ppb Ir and 143.3 ppm Ni. Proportions of the fractionated MSS are assumed to be 0.01, 0.015, 0.02, 0.025, 0.03 and 0.035, respectively. "Residual liquid 1/2" and "cumulate 1/2" represent the trends of the residual liquid and MSS cumulate of the initial sulfide liquid 1anf 2, respectively.

0.015, 0.02, 0.025, 0.03 and 0.035, respectively. Fig. 9A and B shows that either the densely disseminated ores or the net-textured/massive ores are mostly plotted between the trends of MSS cumulates and residual liquids of initial sulfide liquid 1 and 2. The plots show that composition variations of the sulfide ores are not only associated with differentiation of the sulfide liquids but also mixture between differentiated liquid and crystalized MSS and/or among the sulfide liquids segregated from variably PGE-depleted parental magmas. Fractional crystallization of olivine, pyroxene and chromite could decrease IPGE abundances of basaltic magma and slightly elevate Pd in the magma. Therefore, PGE abundances of the initial sulfide liquids segregated from the parental magma could be synergistically affected. However, such effect is not been considered in the modelling calculations because compositions of the parental magmas and proportions of olivine, pyroxene and chromite for each complex hosting the deposit should be various but unknow. In view of buoyancy, basaltic magma containing < 5% sulfide droplets is less dense than normal crustal rocks and could move upward (Barnes et al., 2016). The formation of a large Ni-Cu sulfide deposit need a great amount basaltic magma carrying < 5% sulfides to pass through the magma chamber and a long-lived magma conduit system is necessary (Lightfoot and Evans-Lamswood, 2015). Mixing and remobilization of the sulfide liquids are inevitable during ascending of different pulses of magma.

In the Tulaergen deposit, the Fe-rich and Cu-rich massive ores occur as veins within the ultramafic dyke and emplaced in the volcanic wall rocks, respectively (Zhao et al., 2019). High Pd/Ir and Ni/Ir values indicate that they are the results of highly differentiated sulfide liquids (Fig. 9B). However, the Tulaergen sulfide mineralized ultramafic dyke is only ~ 740 m long and 30 ~ 50 m thick (Fig. 2E) (Wang et al., 2022). The Fe-rich and Cu-rich massive ores were most likely formed by downward percolation of differentiated sulfide liquids in the magma conduit before completely solidification of the sulfides (Barnes et al., 2016; Holwell et al., 2022). Analogously, downward propagation of sulfide liquids formed the massive sulfide veins within the mafic dykes emplaced in country rock below the Reid Brook Chamber hosting large ore bodies at Voisey's Bay (Canada) (Li et al., 2000; Naldrett and Li, 2007). Similar phenomena were also recognized in the Jinchuan deposit in NW China, where Cu-rich massive orebody was discovered in the Proterozoic metamorphic rocks beneath the major orebody (Chen et al., 2013; Yang et al., 2018).

6.5. Decoupling between Pt and Pd

As shown in Fig. 5, the densely disseminated and net-textured/massive ores from the deposits in the Huangshan-Jingerquan metallogenic belt display larger variation in $Pt_{[100]}$ than $Pd_{[100]}$. Although the sulfide ores display a positive correlation between $Pd_{[100]}$ and Pd/Ir, they are remarkably scattered in the diagram of $Pt_{[100]}$ against Pd/Ir (Fig. 8B, C). The Tulaergen Cu-rich massive ores display the largest Pd/Ir values and extremely large variation in $Pt_{[100]}$ and moderately variable $Pd_{[100]}$, while the sulfide ores from the Huangshannan deposit have moderate Pd/Ir values but the largest range of $Pt_{[100]}$ values. These phenomena indicate decoupling between Pt and Pd, which cannot be completely explained by variable Pt concentrations in initial sulfide liquid, differentiation of sulfide liquid and reaction with basaltic magmas. Decoupling between Pt and Pd was also discovered in komatiite-related Ni sulfide deposit, western Australia, and interpreted as the result of hydrothermal alteration (Barnes and Liu, 2012). The hydrothermal remobilizations of Pd and Pt were also recognized in the Jinchuan Ni-Cu-(PGE) sulfide deposit, NW China (Song et al., 2009b; Chen et al., 2013; Prichard et al., 2013; Yang et al., 2018).

Thermodynamic modeling suggests that Pd is commonly more soluble and mobile than Pt as chloride and bisulfide complexes in acidic-neutral solutions under reduced and moderate oxidation condition at 300 °C (Barnes and Liu, 2012). Nugget effects is another factor possibly resulting in large variation of Pt due to heterogeneous distribution of tiny particles rich in Pt in the ores (Barnes et al., 2022). Therefore, decoupling between Pt and Pd in the Tulaergen Cu-rich massive ores

may be associated with differentiation between Pt and Pd during hydrothermal alteration and/or nugget effect (Fig. 8B, C).

7. Mechanism of sulfide mineralization

Song et al. (2021) proposed that the mineralized ultramafic dykes and complexes (Telaergen, Xiangshan and Hulu) in the middle Devonian strata represented magma conduit at deep levels, whereas the stratiform and lenticular orebodies in the large mafic–ultramafic complexes (Huangshan, Huangshandong, Huangshannan, Tudun) in the late Carboniferous strata is the representatives of magma chambers at shallow depths. The sulfides were transported by batches of basaltic magmas from deeper levels and deposited in the dykes and complexes, respectively (Deng et al., 2022).

Sulfide segregation, migration and mixing in magmatic plumbing system along the Hunagshan-Jingerquan belt can be outlined by cartoons in Fig. 10. Olivine-free and sulfide-poor gabbro dykes and sills in Devonian strata were resulted from 380–300 Ma basaltic magmatism in subduction period (Fig. 10A, Wang et al., 2014; Song et al., 2021). In early stage of post collision, the basaltic magmas ascent along the pre-existing fracture network (Fig. 10B). The PGE depleted primary basaltic magmas were generated from upwelling asthenospheric mantle containing remnant sulfides. Reaction with early segregated sulfides in deep levels of the crust could make the basaltic magma more PGE-depleted. Meanwhile, fractionation of mafic minerals may result in differentiation between IPGE and Pd and slightly elevation of Pd/Ir ratio in the basaltic magmas (Fig. 10B). Assimilation of sulfide-bearing crustal rocks led to segregation of sulfide liquids from the basaltic magmas. Thus, the initial sulfide liquids have varied abundances of PGE and values of Pd/Ir and Cu/Pd (Figs. 5 and 7).

The sulfide liquids experienced differentiation in deep levels could be disturbed and carried upward by recharged magmas to widen parts along pathways of the magmas to form sulfide orebodies in dykes or sills in the middle Devonian strata (e.g. Tulaergen and Hulu) (Fig. 2E, F, G, 10B). The differentiated sulfide liquids could percolate downward to form massive sulfide veins within the disseminated orebodies or extending to wall-rock (Fig. 10B). More sulfides were unceasingly carried by ascending basaltic magmas to large magma chambers at shallow depths and deposited to form stratiform or lenticular sulfide orebodies in the Huangshan, Huangshandong and Huangshannan mafic–ultramafic complexes within the late Carboniferous strata (Fig. 2A, B, C, 10B).

8. Conclusions

The magmatic Ni-Cu sulfide deposits along the Huangshan-Jingerquan metallogenic belt have low PGE tenors due to PGE-depleted parental basaltic magma.

Possible reasons of PGE-depletion of the parental magma are sulfide retention in the mantle sources during partial melting and/or reaction with sulfides in the lower crust on the ascending pathway of the magma.

Fractional crystallization of mafic minerals prior to sulfide segregation resulted in differentiation between IPGE and PPGE in the parental magmas.

Compositional variations of Ni, Cu and PGE of the sulfide ores from the deposits are associated with segregation of sulfide liquids from fractionated parental magmas under variable R factor, differentiation and mixing of the sulfide liquids, as well as reaction with recharged basaltic magmas on the pathway upward.

The sulfides were carried by ascending basaltic magma and settled down in mafic–ultramafic dykes and large complexes in deep and shallow levels, respectively, along the magma plumbing system.

Declaration of Competing Interest

The authors declare that they have no known competing financial interests or personal relationships that could have appeared to influence

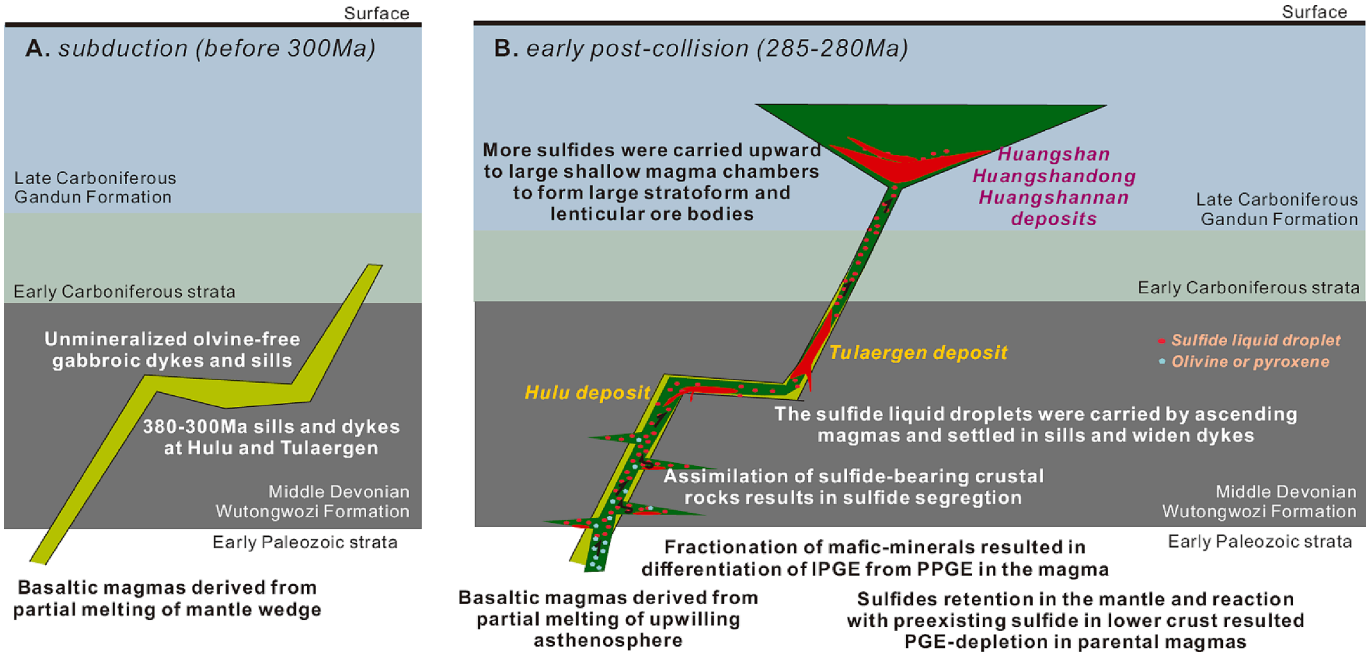

Fig. 10. Cartoons illustrating basaltic magma evolution and sulfide mineralization along magma plumbing system in the Huangshan-Jinerquan Ni-Cu metallogeic belt (after Song et al., 2021; Deng et al., 2022). A. Subduction period: basaltic magmas derived from mantle wedge formed unmineralized olivine-free gabbroic sills and dykes in the Middle Devonian Wutongwozi Formation. B. Early stage of post-collision: basaltic magmas derived from unwilling asthenosphere ascend along the preexisting pathways. Retention of sulfides in the mantle source as well as reaction between the magma and possible preexisting sulfides in the bases of the crust could result in PGE-depletion of the basltic magmas. Fractional crystallization of mafic minerals cause variations of PGE compositions and Pd/Ir ratios of the magma. Addition of sulfur during assimilation of crustal rocks resulting in sulfide segregation at deep levels. The sulfides carried by ascending magma concentrated in dykes and sills within the Wutongwozi Formation and experienced differentiation, mixing and remobilization. More sulfides were transported to large magma chambers within the Gandun Formation at shallow depths to form large stratiform and lenticular ore bodies in large mafic–ultramafic complexes.

the work reported in this paper.

Data availability

all of the data used in this paper have been published and listed in the Appendix tables

Acknowledgements

This study was financially supported by NSFC research grants (42121003, 41630316, 41772067, 41873031 and U1803113).

Appendix A. Supplementary data

Supplementary data to this article can be found online at https://doi.org/10.1016/j.oregeorev.2023.105465.

References

Arndt, N.T., Lesher, C.M., Czamanske, G.K., 2005. Mantle derived magmas and magmatic Ni-Cu-PGE deposits. Econ. Geol. 100th Anniversary Volume, 5–24.

Barnes, S.-J., Maier, W.D., 1999. The fractionation of Ni, Cu, and the noble metals in silicate and sulphide liquids. In: Keays RR, Lesher CM, Lightfoot PC, Farrow CEG (Ed.) Dynamic processes in magmatic ore deposits and their application to mineral exploration, Short course notes, 13, pp. 69-106.

Barnes, S.J., Liu, W., 2012. Pt and Pd mobility in hydrothermal fluids: evidence from komatiites and from thermodynamic modelling. Ore Geol. Rev. 44, 49–58.

Barnes, S.J., Makkonen, H.V., Dowling, S.E., Hill, R.E.T., Peltonen, P., 2009. The 1.88 Ga Kotalahti and Vammala Nickel Belts, Finland: geochemistry of the mafic and ultramafic metavolcanic rocks. Bulletin Geology Society Finland 81 (2), 103–141.

Barnes, S.J., Cruden, A.R., Arndt, N., Saumur, B.M., 2016. The mineral system approach applied to magmatic Ni-Cu-PGE sulphide deposits. Ore Geol. Rev. 76, 296–316.

Barnes, S.J., Stanley, C.R., Taranovic, V., 2022. Compositions and Ni-Cu-PGE tenors of Nova-Bollinger ores with implications for the origin of Pt anomalies in PGE-poor massive sulfides. Econ. Geol. 117, 1687-1707.

Barnes, S.-J., Makovicky, E., Makovicky, M., Hansen, J.R., Moller, S.K., 1997. Partition coefficients for Ni, Cu, Pd, Pt, Rh and Ir between monosulfide solid solution and sulfide liquid and the implication for the formation of compositionally zoned Ni-Cu sulfide bodies by fractional crystallization of sulfide liquid. Can. J. Earth Sci. 34, 366–374.

Campbell, I.H., Naldrett, A.J., 1979. The influence of silicate: sulfide ratios on the geochemistry of magmatic sulfides. Econ. Geol. 74, 1503–1506.

Chai, F., Zhang, Z., Mao, J., Dong, L., Zhang, Z., Wu, H., 2008. Geology, petrology and geochemistry of the Baishiquan Ni-Cu-bearing mafic-ultramafic intrusions in Xinjiang. NW China: implications for tectonics and genesis of ores: Journal of Asian Earth Sciences 32 (2-4), 218–235.

Chen, L.-M., Song, X.-Y., Keays, R.R., Tian, Y.-L., Wang, Y.-S., Deng, Y.-F., Xiao, J.-F., 2013. Segregation and fractionation of magmatic Ni-Cu-PGE sulfides in the western Jinchuan intrusion, northwestern China: insights from platinum group element geochemistry. Econ. Geol. 108 (8), 1793–1811.

Chen, Z., Xiao, W.-J., Windley, B.F., Schulmann, K., Mao, Q., Zhang, Z., Zhang, J., Deng, C., Song, S., 2019. Composition, provenance and tectonic setting of the Southern Kangurtag accretionary complex in the Eastern Tianshan, NW China: Implications for the late Paleozoic evolution of the North Tianshan Ocean. Tectonics 38, 2779–2802.

Chong, J., Fiorentini, M.L., Holwell, D.A., Moroni, M., Blanks, D.E., Dering, G.M., Davis, A., Ferrari, E., 2021. Magmatic cannibalisation of a Permo-Triassic Ni-Cu-PGE-(Au-Te) system during the breakup of Pangea - Implications for craton margin metal and volatile transfer in the lower crust. Lithos 388-389, 106079.

Crockett, J.H., 2002. Platinum group element geochemistry of mafic and ultramafic rocks. In: Cabri LJ (Ed.) The Geology, Geochemistry, Mineralogy and Mineral Beneficiation of Platinum-Group Elements, Spec. v. 54, 177-210.

Deng, Y.-F., Song, X.-Y., Xie, W., Chen, L.-M., Yu, S.-Y., Yuan, F., Hollings, P., Wei, S., 2022. The Role of external sulfur in triggering sulfide immiscibility at depth: Evidence from the Huangshan-Jingerquan Ni-Cu metallogenic belt, NW China. Econ. Geol. 117, 1867-1879.

Deng, Y.-F., Song, X.-Y., Zhou, T.-F., Yuan, F., Chen, L.-M., Zheng, W.-Q., 2012. Correlations between Fo number and Ni content of olivine of the Huangshandong intrusion, eastern Tianshan, Xinjiang, and the genetic significances. Acta Petrol. Sinica 28, 2224–2234 in Chinese with English abstract.

Deng, Y.-F., Song, X.-Y., Chen, L.-M., Zhou, T.-F., Pirajno, F., Yuan, F., Xie, W., Zhang, D.-Y., 2014. Geochemistry of the Huangshandong Ni–Cu deposit in northwestern China: Implications for the formation of magmatic sulfide mineralization in orogenic belts. Ore Geol. Rev. 56, 181–198.

Deng, Y.-F., Song, X.-Y., Hollings, P., Zhou, T., Yuan, F., Chen, L.-M., Zhang, D.-Y., 2015. Role of asthenosphere and lithosphere in the genesis of the Early Permian Huangshan mafic–ultramafic intrusion in the Northern Tianshan, NW China. Lithos 227, 241–254.

Deng, Y.-F., Song, X.-Y., Hollings, P., Chen, L.-M., Zhou, T., Yuan, F., Xie, W., Zhang, D., Zhao, B., 2017. Lithological and geochemical constraints on the magma conduit systems of the Huangshan Ni–Cu sulfide deposit. NW China. Mineral. Deposita 52 (6), 845–862.

Deng, Y.-F., Song, X.-Y., Xie, W., Yuan, F., Zhao, Z.-M., Wei, S., Zhu, J.-J., Kang, J., Wang, K.-Y., Liang, Q.-L., Chen, L.-M., Yu, S.-Y., 2021. Determination of sedimentary ages of strata in the Huangshan-Jingerquan mineralization belt and its geological significance. Acta Geol. Sinica 95, 362–376 in Chinese with English abstract.

Ely, J.C., Neal, C.R., 2002. Method of data reduction and uncertainty estimation for platinum–group element data using inductively coupled plasma–mass spectrometry. Geostand. Geoanal. Res. 26, 31–39.

Fiorentini, M.L., LaFlamme, C., Denyszyn, S., Mole, D., Maas, R., Locmelis, M., Caruso, S., Bui, T.-H., 2018. Post-collisional alkaline magmatism as gateway for metal and sulfur enrichment of the continental lower crust. Geochim. Cosmochim. Acta 223, 175–197.

Fleet, M.E., Chryssoulis, S.L., Stone, W.E., Weisener, C.G., 1993. Partition of platinum–group elements and Au in the Fe–Ni–Cu–S system: experiments on the fractional crystallization of sulfide melt. Contrib. Mineral. Petrol. 115, 36–44.

Fleet, M.E., Crocket, J.H., Liu, M., Stone, W.E., 1999a. Laboratory partitioning of platinum–group elements (PGE) and gold with application to magmatic sulfide–PGE deposits. Lithos 47 (1-2), 127–142.

Fleet, M.E., Liu, M., Crocket, J.H., 1999b. Partitioning of trace amounts of highly siderophile elements in the Fe–Ni–S system and their fractionation in nature. Geochim. Cosmochim. Acta 63 (17), 2611–2622.

Gao, J.-F., Zhou, M.-F., Lightfoot, P.C., Wang, C.Y., Qi, L., Sun, M., 2013. Sulfide saturation and magma emplacement in the formation of the Permian Huangshandong Ni–Cu sulfide deposit, Xinjiang, NW China. Econ. Geol. 108, 1833–1848.

Han, C.-M., Xiao, W.-J., Zhao, G.-C., Su, B.-X., Saky, P.A., Ao, S.-J., Wan, B., Zhang, J., Zhang, Z.-Y., 2013. SIMS U-Pb zircon dating and Re-Os isotopic analysis of the Hulu Cu-Ni deposit, eastern Tianshan, Central Asian Orogenic Belt, and its geological significance. Journal of Geology 58, 251–270.

Han, Y., Zhao, G., 2018. Final amalgamation of the Tianshan and Junggar orogenic collage in the southwestern Central Asian Orogenic Belt: Constraints on the closure of the Palo-Asian Ocean. Earth-Science Review 186, 129–152.

Hill, E., Wood, B.J., Blundy, J.D., 2000. The effect of Ca-Tschermaks component on trace element partitioning between clinopyroxene and silicate melt. Lithos 53 (3-4), 203–215.

Holwell, D.A., Fiorentini, M.L., McDonald, I., Lu, Y., Giuliani, A., Smith, D.J., Keith, M., Locmelis, M., 2019. A metasomatized lithospheric mantle control on the metallogenic signature of post-subduction magmatism. Nature Com. 10, 3511.

Holwell, D.A., Fiorentini, M.L., Knott, T.R., McDonald, I., Blanks, D.E., McCuaig, T.C., Gorczyk, W., 2022. Mobilisation of deep crustal sulfide melts as a first order control on upper lithospheric metallogeny. Nature Com. 13, 573.

Jiang, C., Qian, Z., Zhang, J., Sun, T., Xu, G., Meng, D., 2014. Characteristics and genetic significances of olivine from Xiangshan complex in eastern Tianshan, Xinjiang. Geoscience 28, 478–488 in Chinese with English abstract.

Keays, R.R., 1995. The role of komatiitic and picritic magmatism and S–saturation in the formation of ore deposits. Lithos 34 (1-3), 1–18.

Kelemen, P.B., 1990. Reaction between ultramafic rock and fractionating basaltic magma I. Phase relations, the origin of calc–alkaline magma series, and the formation of discordant dunite. J. Petrol. 31 (1), 51–98.

Le Vaillant, M., Barnes, S.J., Mole, D.R., Fiorentini, M.L., Laflamme, C., Denyszyn, S.W., Austin, J., Patterson, B., Godel, B., Hicks, J., Mao, Y.-J., Neaud, A., 2020. Multidisciplinary study of a complex magmatic system: The Savannah Ni-Cu-Co Camp. Western Australia. Ore Geology Reviews 117, 103292.

Li, C., Lightfoot, P.C., Amelin, Y., Naldrett, A.J., 2000. Contrasting petrological and geochemical relationships in the voisey's bay and mushuau intrusions, labrador, Canada: implications for ore genesis. Econ. Geol. 95 (4), 771–799.

Li, C., Zhang, Z., Li, W., Wang, Y., Sun, T., Ripley, E.M., 2015. Geochronology, petrology and Hf-S isotope geochemistry of the newly discovered Xiarihamu magmatic Ni-Cu sulfide deposit in the Qinghai-Tibet plateau, western China. Lithos 216–217, 224–240.

Lightfoot, P.C., Evans-Lamswood, D., 2015. Structural controls on the primary distribution of mafific–ultramafic intrusions containing Ni-Cu-Co-(PGE) sulfide mineralization in the roots of large igneous provinces. Ore Geol. Rev. 64, 354–386.

Lightfoot, P.C., Hawkesworth, C.J., Olshefsky, K., Green, T., Doherty, W., Keays, R.R., 1997. Geochemistry of Tertiary tholeiites and picrites from Qeqertarssuaq (Disko Island) and Nuussuaq, West Greenland with implications for the mineral potential of comagmatic intrusions. Contrib. Mineral. Petrol. 128 (2-3), 139–163.

Liu, Y., Brenan, J., 2015. Partitioning of platinum–group elements (PGE) and chalcogens (Se, Te, As, Sb, Bi) between monosulfide–solid solution (MSS), intermediate solid solution (ISS) and sulfide liquid at controlled f_{O2}–f_{S2} conditions. Geochim. Cosmochim. Acta 159, 139–161.

Liu, Y., Lv, X., Mei, W., Hui, W., 2012. Compositions of olivine from the mafic-ultramafic complexes in eastern Tianshan, Xinjiang and implications to petrogenesus: Examples from Huangshandong and Tulargen complexes. Geochimica 41, 78–88 in Chinese with Eglish abstract.

Maier, W.D., Barnes, S.-J., Chinyepi, G., Barton, J.M., Eglington, B., Setshedi, I., 2008. The composition of magmatic Ni-Cu-(PGE) sulfide deposits in the Tati and Selebi-Phikwe belts of eastern Botswana. Miner. Deposita 43 (1), 37–60.

Maier, W.D., Smithies, R.H., Spaggiari, C.V., Barnes, S.J., Kirkland, C.L., Yang, S., Lahaye, Y., Kiddie, O., MacRae, C., 2016. Petrogenesis and Ni-Cu sulphide potential of mafic-ultramafic rocks in the Mesoproterozoic Fraser Zone within the Albany-Fraser Orogen, Western Australia. Precambr. Res. 281, 27–46.

Mao, J.W., Pirajno, F., Zhang, Z.H., Chai, F.M., Wu, H., Chen, S.P., Cheng, L.S., Yang, J. M., Zhang, C.Q., 2008. A review of the Cu-Ni sulphide deposits in the Chinese

Tianshan and Altay orogens (Xinjiang Autonomous Region, NW China): Principal characteristics and ore-forming processes. J. Asian Earth Sci. 32 (2-4), 184–203.
Mao, Y.J., Qin, K.Z., Li, C., Xue, S., C., Ripley, E.M., 2014. Petrogenesis and ore genesis of the Permian Huangshanxi sulfide ore–bearing mafic–ultramafic intrusion in the Central Asian orogenic belt, western China. Lithos 200–201, 111–125.
Mao, Y.-J., Qin, K.-Z., Li, C., Tang, D.-M., 2015. A modified genetic model for the Huangshandong magmatic sulfide deposit in the Central Asian Orogenic Belt, Xinjiang, western China. Mineral. Deposita 50 (1), 65–82.
Mao, Y.J., Qin, K.Z., Barnes, S.J., Tang, D.M., Xue, S.C., Vaillant, M.L., 2017. Genesis of the Huangshannan high–Ni tenor magmatic sulfide deposit in the Eastern Tianshan, northwest China: constraints from PGE geochemistry and Os-S isotopes. Ore Geol. Rev. 90, 591–606.
Mungall, J.E., Brenan, J.M., 2014. Partitioning of platinum–group elements and Au between sulfide liquid and basalt and the origins of mantle–crust fractionation of the chalcophile elements. Geochim. Cosmochim. Acta 125, 265–289.
Naldrett, A.J., Li, C., 2007. The Voisey's Bay deposit, Labrador, Canada. In: Goodfellow WD (Ed.) Mineral Deposits of Canada: A Synthesis of Major Deposit-Types, District Metallogeny, the Evolution of Geological Provinces, and Exploration Methods, Geological Association of Canada, Mineral Deposits Division, Special Publication No. 5, pp 387-407.
Pina, R., Romeo, I., Ortega, L., Lunar, R., Capote, R., Gervilla, F., Tejero, R., Quesada, C., 2010. Origin and emplacement of the Aguablanca magmatic Ni-Cu-(PGE) sulfide deposit, SW Iberia: A multidisciplinary approach. Geol. Soc. Am. Bull. 122 (5-6), 915–925.
Pirajno, F., Mao, J., Zhang, Z., Zhang, Z., Chai, F., 2008. The association of mafic–ultramafic intrusions and A-type magmatism in the Tianshan and Altay orogens, NW China: Implications for geodynamic evolution and potential for the discovery of new ore deposits. Journal Asian Earth Sciences 32 (2-4), 165–183.
Prichard, H.M., Knight, R.D., Fisher, P.C., McDonald, I., Zhou, M.-F., Wang, C.Y., 2013. Distribution of platinum–group elements in magmatic and altered ores in the Jinchuan intrusion, China: an example of selenium remobilization by postmagmatic fluids. Mineral. Deposita 48 (6), 767–786.
Puchtel, I.S., Humayun, M., 2001. Platinum Group Element Fractionation in a Komatiitic Basalt Lava Lake. Geochim. Cosmochim. Acta 65 (17), 2979–2993.
Qin, K.Z., Su, B.X., Sakyi, P.A., Tang, D.M., Li, X.H., Sun, H., Xiao, Q.H., Liu, P.P., 2011. SIMS zircon U-Pb geochronology and Sr-Nd isotopes of Ni-Cu bearing mafic–ultramafic intrusions in Eastern Tianshan and Beishan in correlation with flood basalts in Tarim Basin (NW China): constraints on a ca. 280 Ma mantle plume. Am. J. Sci. 311 (3), 237–260.
Rehkämper, M., Halliday, A.N., Fitton, J.G., Lee, D.C., Wieneke, M., Arndt, N.T., 1999. Ir, Ru, Pt, and Pd in basalts and komatiites: New constraints for the geochemical behavior of the platinum-group elements in the mantle. Geochim. Cosmochim. Acta 63 (22), 3915–3934.
Righter, K., Campbell, A.J., Humayun, M., Hervig, R.L., 2004. Partitioning of Ru, Rh, Pd, Re, Ir, and Au between Cr–bearing spinel, olivine, pyroxene and silicate melts. Geochim. Cosmochim. Acta 68 (4), 867–880.
Robertson, J.C., Barnes, S.J., Le Vaillant, M., 2015. Dynamics of magmatic sulphide droplets during transport in silicate melts and implications for magmatic sulphide ore formation. J. Petrol. 56 (12), 2445–2472.
San, J.Z., Tian, B., Lei, J.W., Kang, F., Qin, K.Z., Xu, X.W., 2003. The discovery of magmatic Cu-Ni deposit of Tulaergen with whole-rock mineralization at eastern Tianshan, Xinjiang. Mineral Deposit 3, 265–270 in Chinese with English abstract.
Şengör, A.M.C., Natal'in, B.A., Burtman, V.S., 1993. Evolution of the Altaid tectonic collage and Paleozoic crustal growth in Asia. Nature 364, 299–307.
Song, X.-Y., Li, X.-R., 2009. Geochemistry of the Kalatongke Ni-Cu-(PGE) sulfifide deposit, NW China: implications for the formation of magmatic sulfide mineralization in a post–collisional environment. Mineral. Deposita 44, 303–327.
Song, X.-Y., Qi, H.-W., Robinson, P.T., Zhou, M.-F., Cao, Z.-M., Chen, L.-M., 2008. Melting of the subcontinental lithospheric mantle by the Emeishan mantle plume; evidence from the basal alkaline basalts in Dongchuan, Yunnan, Southwestern China. Lithos 100 (1-4), 93–111.
Song, X.-Y., Keays, R.R., Xiao, L., Qi, H.-W., Ihlenfeld, C., 2009a. Platinum-group element geochemistry of the continental flood basalts in the central Emeisihan Large Igneous Province, SW China. Chem. Geol. 262 (3-4), 246–261.
Song, X.-Y., Keays, R.R., Zhou, M.-F., Qi, L., Ihlenfeld, C., Xiao, J.-F., 2009b. Siderophile and chalcophile elemental constraints on the origin of the Jinchuan Ni-Cu-(PGE) sulfifide deposit. NW China. Geochim. Cosmochim. Acta 73, 404–424.
Song, X.-Y., Xie, W., Deng, Y.-F., Crawford, A.J., Zheng, W.-Q., Zhou, G.-F., Deng, G., Cheng, S.-L., Li, J., 2011. Slab break-off and the formation of Permian mafic-ultramafic intrusions in southern margin of Central Asian Orogenic Belt, Xinjiang, NW China. Lithos 127 (1-2), 128–143.
Shi, Y., Wang, Y.W., Wang, J.B., Zhao, L.T., Xie, H.J., Long, L.L., Zou, T., Li, D.D., Zhou, G.C., 2018. Physicochemical control of the Early Permian Xiangshan Fe-Ti oxide deposit in Eastern Tianshan (Xinjiang), NW China. Journal of Earth Sciences 29, 520–536.
Song, X.-Y., Chen, L.-M., Deng, Y.-F., Xie, W., 2013. Syncollisional tholeiitic magmatism induced by asthenosphere upwelling owing to slab detachment at the southern margin of the Central Asian Orogenic Belt. J. Geol. Soc. 170 (6), 941–950.
Song, X.-Y., Yi, J.-N., Chen, L.-M., She, Y.-W., Liu, C.-Z., Dang, X.-Y., Yang, Q.-A., Wu, S.-K., 2016. The Giant Xiarihamu Ni-Co Sulfide Deposit in the East Kunlun Orogenic Belt, Northern Tibet Plateau, China. Econ. Geol. 111 (1), 29–55.
Song, X.-Y., Deng, Y.-F., Xie, W., Yi, J.-N., Fu, B., Chen, L.-M., Yu, S.-Y., Zheng, W.-Q., Liang, Q.-L., 2021. Prolonged basaltic magmatism and short-lived magmatic sulfide mineralization in orogenic belt. Lithos 390–391, 106114.
Sun, T., Qian, Z.-Z., Deng, Y.-F., Li, C., Song, X.-Y., Tang, Q., 2013. PGE and isotope (Hf-Sr-Nd-Pb) constraints on the origin of the Huangshandong magmatic Ni-Cu sulfide deposit in the Central Asian Orogenic Belt, Northwestern China. Econ. Geol. 108 (8), 1849–1864.
Tang, D., Qin, K., Su, B., Sakyi, P.A., Mao, Y., Xue, S., 2014. Petrogenesis and mineralization of the Hulu Ni–Cu sulphide deposit in Xinjiang, NW China: constraints from Sr–Nd isotopic and PGE compositions. Intern. Geol. Rev. 56 (6), 711–733.
Wang, B., Cluzel, D., Jahn, B.-m., Shu, L., Chen, Y., Zhai, Y., Branquet, Y., Barbanson, L., Sizaret, S., 2014. Late Paleozoic pre- and syn-kinematic plutons of the Kangguer-Huangshan shear zone: Inference on the tectonic evolution of the Eastern Chinese North Tianshan. Am. J. Sci. 314 (1), 43–79.
Wang, M.F., Guo, X., Michalak, P.P., Xia, Q., Xiao, F., Wang, W., Liu, K., 2015. Origin of the Tudun Cu–Ni sulfifide deposit in the eastern Tianshan, NW China: Constraints on the geochemistry of platinum group elements. Ore Geol. Rev. 64, 445–454.
Wang, Y., Lv, X., Liu, Y., 2018. Petrogenesis and Ni-Cu-Co sulfide formation of mafic enclaves in Tulaergen mafic–ultramafic intrusive rocks, Eastern Tianshan, Northwest China: implications for liquid immiscibility and hydrothermal remobilization of platinum-group elements. Econ. Geol. 113, 1795–1816.
Wang, Y., Li, C., Li, W., Zhang, Z., Ripley, E.M., Gao, Y., Zhang, J., 2022. Geology and geochemistry of the Tulaergen conduit-style magmatic Ni-Cu sulfide deposit in the Central Asian Orogenic Belt, northwestern China. Mineral. Deposita 57 (2), 319–342.
Wang, J.B., Wang, Y.W., He, Z.J., 2006. Ore deposits as guide to the tectonic evolution in the East Tianshan Mountains, NW China. Geol. China 33, 461–469 in Chinese with English abstract.
Xia, M.-Z., Jiang, C.-Y., Li, C., Xia, Z.-D., 2013. Characteristics of a newly discovered Ni-Cu sulfide deposit hosted in the Poyi ultramafic intrusion, Tarim Craton, NW China. Econ. Geol. 108 (8), 1865–1878.
Xiao, W., Windley, B.F., Allen, M.B., Han, C., 2013. Paleozoic multiple accretionary and collisional tectonics of the Chinese Tianshan orogenic collage. Gond. Res. 23 (4), 1316–1341.
Xiao, W., Windley, B.F., Sun, S., Li, J., Huang, B., Han, C., Yuan, C., Sun, M., Chen, H., 2015. A Tale of amalgamation of Three Permo-Triassic Collage Systems in Central Asia: Oroclines, Sutures, and Terminal Accretion. Annual Rev. Earth and Planet. Sci. 43 (1), 477–507.
Xie, W., Song, X.Y., Deng, Y.F., Wang, Y.S., Ba, D.H., Zheng, W.Q., Li, X.B., 2012. Geochemistry and petrogenetic implications of a Late Devonian mafic-ultramafic intrusion at the southern margin of the Central Asian Orogenic Belt. Lithos 144, 209–230.
Xie, W., Song, X.-Y., Chen, L.-M., Deng, Y.-F., Zheng, W.-Q., Wang, Y.-S., Ba, D.-H., Zhang, X.-Q., Luan, Y., 2014. Geochemistry insights on the genesis of the subduction–related Heishan magmatic Ni-Cu-(PGE) deposit in Gansu, NW China, at the Southern margin of the Central Asian Orogenic Belt. Econ. Geol. 109, 1563–1583.
Xue, S., Qin, K., Li, C., Tang, D., Mao, Y., Qi, L., Ripley, E.M., 2016. Geochronological, petrological, and geochemical constraints on Ni-Cu sulfide mineralization in the Poyi ultramafic-troctolitic intrusion in the northeast rim of the Tarim Craton, Western China. Econ. Geol. 111 (6), 1465–1484.
Yang, S., Yang, G., Qu, W., Du, A., Hanski, E., Lahaye, Y., Chen, J., 2018. Pt-Os isotopic constraints on the age of hydrothermal overprinting on the Jinchuan Ni-Cu-PGE deposit. China. Mineral. Deposita 53 (6), 757–774.
Zhang, M., Li, C., Fu, P., Hu, P., Ripley, E.M., 2011. The Permian Huangshanxi Cu-Ni deposit in western China: intrusive-extrusive association, ore genesis, and exploration implications. Mineral. Deposita 46 (2), 153–170.
Zhang, Z.C., Mao, J.W., Chai, F.M., Yan, S.H., Chen, B.L., Pirajno, F., 2009a. Geochemistry of the Permian Kalatongke mafic intrusions, Northern Xinjiang, NW China, Implications for the Genesis of the Magmatic Ni-Cu Sulfide Deposit. Econ. Geol. 104 (2), 185–203.
Zhang, Z.C., Mao, J.W., Saunders, A.D., Ai, Y., Li, Y., Zhao, L., 2009b. Petrogenetic modeling of three mafic-ultramafic layered intrusions in the Emeishan large igneous province, SW China, based on isotopic and bulk chemical constraints. Lithos 113 (3–4), 369–392.
Zhao, Y., Xue, C.-J., Symons, D.T.A., Zhao, X.-B., Zhang, G.-Z., Yang, Y.-Q., Zu, B., 2018. Temporal variations in the mantle source beneath the Eastern Tianshan nickel belt and implications for Ni-Cu mineralization potential. Lithos 314-315, 597–616.
Zhao, Y., Xue, C., Zhao, X., Yang, Y., Ke, J., 2015. Magmatic Cu–Ni sulfide mineralization of the Huangshannan mafic–untramafic intrusion, Eastern Tianshan. China. J. Asian Earth Sci. 105, 155–172.
Zhao, Y., Xue, C., Zhao, X., Yang, Y.Q., Ke, J., Zu, B., Zhang, G.Z., 2016. Origin of anomalously Ni–rich parental magmas and genesis of the Huangshannan Ni-Cu sulfide deposit, Central Asian Orogenic Belt. Northwestern China. Ore Geol. Rev. 77, 57–71.
Zhao, Y., Xue, C.-J., Liu, S.-A., Mathur, R., Zhao, X.-B., Yang, Y.-Q., Dai, J.-F., Man, R.-H., Liu, X.-M., 2019. Redox reactions control Cu and Fe isotope fractionation in a magmatic Ni–Cu mineralization system. Geochim. Cosmochim. Acta 249, 42–58.
Zhou, M.-F., Michael Lesher, C., Yang, Z., Li, J., Sun, M., 2004. Geochemistry and petrogenesis of 270 Ma Ni-Cu-(PGE) sulfide-bearing mafic intrusions in the Huangshan District, eastern Xinjiang, northwest China; implications for the tectonic evolution of the Central Asian orogenic belt. Chem. Geol. 209 (3-4), 233–257.